

2. EXPLANATORY NOTES¹

Shipboard Scientific Party²

INTRODUCTION

This chapter explains the techniques and procedures used during Leg 189 to help document the basis for our preliminary scientific conclusions and to provide the interested investigator with the information needed to select samples for further analysis. This information concerns only shipboard operations and analyses described in the site reports in the Leg 189 *Initial Reports* volume of the *Proceedings of the Ocean Drilling Program*. The methods used by various investigators for shore-based analyses of Leg 189 data will be described in the individual scientific contributions published in the *Scientific Results* volume and in publications in various professional journals.

Authorship of Site Chapters

The separate sections of the site chapters were written by the following shipboard scientists (authors are listed in alphabetical order; no seniority is implied):

Principal Results: Shipboard Party

Background and Objectives: Exon, Kennett

Operations: Grout, Malone

Lithostratigraphy: Ennyu, Grauert, Nees, Pekar, Pellaton, Robert, Schellenberg, Shevenell

Biostratigraphy: Brinkhuis, Chaproniere, Kelly, McGonigal [N1], Pfuhl, Stickley, Suzuki, Wei

Paleomagnetism: Fuller, Touchard

Composite Depths: Hill, Janecek

Organic Geochemistry: White

Inorganic Geochemistry: Malone, Nürnberg

Physical Properties: Latimer, Röhl

Downhole Measurements: Fothergill, Ninnemann

¹Examples of how to reference the whole or part of this volume.

²Shipboard Scientific Party addresses.

Drilling Characteristics

Information concerning sedimentary stratification in uncored or unrecovered intervals may be inferred from seismic data, wireline-logging results, and an examination of the behavior of the drill string as observed and recorded on the drilling platform. Typically, the harder a layer, the slower and more difficult it is to penetrate. A number of other factors may determine the rate of penetration (ROP), so it is not always possible to relate the drilling time directly to the hardness of the layers.

Drilling Deformation

When cores are split, many show signs of significant sediment disturbance, including the concave-downward appearance of bedding that was originally horizontal, haphazard mixing of lumps of different lithologies (mainly at the tops of cores), fluidization, and flow-in. Core deformation may also occur during retrieval because of changes in pressure and temperature as the core is raised and during cutting and core handling on deck.

Shipboard Scientific Procedures

Numbering of Sites, Holes, Cores, and Samples

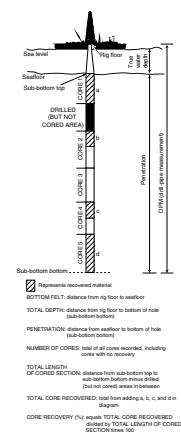
Ocean Drilling Program (ODP) drill sites are numbered consecutively and refer to one or more holes drilled while the ship was positioned over one acoustic beacon. Multiple holes may be drilled at a single site by pulling the drill pipe above the seafloor (out of the hole), moving the ship some distance from the previous hole, and then drilling another hole.

For all ODP drill sites, a letter suffix distinguishes each hole drilled at the same site. The first hole drilled is assigned the site number modified by the suffix "A," the second hole takes the site number and suffix "B," and so forth. Note that this procedure differs slightly from that used by the Deep Sea Drilling Project (DSDP; Sites 1 through 624) but prevents ambiguity between site-and hole-number designations. It is important to distinguish among holes drilled at a site because recovered sediments or rocks from different holes usually do not come from exactly equivalent positions in the stratigraphic column.

The cored interval is measured in meters below seafloor (mbsf). The depth interval assigned to an individual core begins with the depth below the seafloor that the coring operation began and extends to the depth that the coring operation ended (see Fig. F1). Each cored interval is ~9.5 m long, which is the length of a core barrel. Coring intervals may be shorter and may not necessarily be continuous if separated by drilled intervals. In soft sediments, the drill string can be "washed ahead" with the core barrel in place, without recovering sediments. This is achieved by pumping water down the pipe at high pressure to wash the sediment out of the way of the bit and up the space between the drill pipe and the wall of the hole.

Cores taken from a hole are numbered serially from the top of the hole downward. Core numbers and their associated cored intervals ideally are unique in a given hole; however, this may not be true if an interval is cored twice, if the borehole wall caves in, or other hole problems occur. Full recovery for a single core is 9.5 m of rock or sediment contained in a plastic liner (6.6-cm internal diameter) plus ~0.2 m

F1. Coring and depth intervals, p. 38.



(without a plastic liner) in the core catcher (Fig. F2). The core catcher is a device at the bottom of the core barrel that prevents the core from sliding out when the barrel is being retrieved from the hole. In many advanced hydraulic piston corer/extended core barrel (APC/XCB) cores, recovery exceeds the 9.5-m theoretical maximum by as much as 0.60 m (see “Composite Depths,” p. 18). The recovered core in its liner is divided into 1.5-m sections that are numbered serially from the top (Fig. F2). When full recovery is obtained, the sections are numbered from 1 through 7, with the last section generally being shorter than 1.5 m. Rarely, a core may require more than seven sections; this is usually the result of gas expansion having caused voids within some sections. When less than full recovery is obtained, as many sections as are needed to accommodate the length of the core will be recovered; for example, 4 m of core would be divided into two 1.5-m sections and a 1-m section. If cores are fragmented (<100% recovery), sections are numbered serially and intervening sections are noted as void, whether shipboard scientists believe that the fragments were contiguous in situ or not. In rare cases, a section <1.5 m may be cut to preserve features of interest. Sections <1.5 m in length are also sometimes cut when the core liner is severely damaged.

By convention, material recovered from the core catcher is placed immediately below the last section when the core is described and is labeled core catcher (CC); in sedimentary cores, it is treated as a separate section. In cases where material is only recovered in the core catcher, it is assigned the depth of the top of the cored interval (this convention differs from that used in the early days of deep-sea drilling), even though information from the driller or other sources may indicate from what depth it was actually recovered.

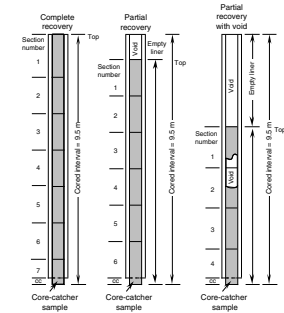
When the recovered core is shorter than the cored interval, the top of the core is equated with the top of the cored interval by convention to achieve consistency when handling analytical data derived from the cores. Samples removed from the cores are designated by distance, measured in centimeters, from the top of the section to the top and bottom of each sample removed from that section. A complete identification number for a sample consists of the following information: leg, site, hole, core number, core type, section number, piece number (for hard rock), and interval in centimeters, measured from the top of the section. For example, a sample identification of “189-1168A-11H-6, 10–12 cm” would be interpreted as representing a sample removed from the interval between 10 and 12 cm below the top of Section 6, Core 11 (H designates that this core was taken by the advanced piston corer) of Hole 1168A during Leg 189. A computer routine is available to calculate depth mbsf from any correctly formulated ODP sample designation.

All ODP core and sample identifiers indicate core type. The following abbreviations are used: H = hydraulic piston core (HPC; also referred to as APC, or advanced hydraulic piston core); X = extended core barrel (XCB); R = rotary core barrel (RCB); W = wash-core recovery; and M = miscellaneous material. APC, XCB, RCB, and W cores were cut during Leg 189.

Core Handling

As soon as a core was retrieved on deck, a sample taken from the core catcher was given to the paleontological laboratory for an initial age assessment. Special care was taken in transferring the core from the drill floor to a long horizontal rack on a catwalk near the core laboratory so

F2. Examples of numbered core sections, p. 39.



that the core did not bend or twist excessively. The core was capped immediately, and gas samples were taken by piercing the core liner at voids, when present, and withdrawing gas into a vacuum tube. Some of the gas samples were stored for shore-based study, but others were analyzed immediately as part of the shipboard safety and pollution-prevention program. Next, the core was marked into section lengths of 150 cm, each section was labeled, and the core was cut into sections. Interstitial water (IW) and whole-round samples were also taken at this time. In addition, headspace gas samples were taken from the end of cut sections on the catwalk and sealed in glass vials for light hydrocarbon analysis. Afterward, each section was sealed at the top and bottom by gluing on color-coded plastic caps: blue to identify the top of a section and clear for its bottom. A yellow cap was placed on the section ends from which a whole-round sample was removed. The caps were usually attached to the liner by coating the end liner and the inside rim of the cap with acetone and then attaching the caps to the liners.

The cores were then carried into the laboratory, where the sections were labeled with an engraver to permanently mark the complete designation of the section. The length of the core in each section and the core-catcher sample were measured to the nearest centimeter. This information was logged into the shipboard Oracle database (Janus).

Whole-round sections from APC and XCB cores were routinely run through the multisensor track (MST) after equilibrating to room temperature, typically ~3–4 hr. The MST includes the gamma-ray attenuation (GRA) bulk densiometer, a compressional wave (*P*-wave) logger, natural gamma-ray emission measurement, and a volume magnetic susceptibility meter. Soft sediments were measured for thermal conductivity before being split lengthwise into working and archive halves. Softer cores were split with a wire. Harder cores were split using a diamond saw. The wire-cut cores were split from the top to bottom so that sediment below the voids or soupy intervals that were sometimes present at the top of Section 1 would not be drawn into the voids.

After splitting, the halves of the core were designated as working and archive halves, respectively. Archive halves were then described visually and run through the Minolta color scanner and the cryogenic magnetometer. Finally, the cores were photographed with both black-and-white and color film, a whole core at a time. Close-up photographs (black-and-white and color) were taken of particular features, as requested by individual scientists, for illustrations in the summary of each site.

The working half of the core was measured first for sonic velocity. After physical properties and paleomagnetic sampling, the working half was sampled for shipboard and shore-based laboratory studies.

Each sample taken either for shipboard or shore-based analysis was logged into the Oracle database (Janus) by the location and the name of the investigator receiving the sample. Records of all of the samples removed are kept in the database and by the curator at ODP headquarters. The extracted samples were sealed in plastic bags and labeled.

Both halves of the core were placed into labeled plastic tubes, which were then sealed and transferred to cold-storage space aboard the drilling vessel. When the leg ended, the cores were transferred from the ship in refrigerated containers to cold storage at the ODP core repository in College Station, Texas, USA.

LITHOSTRATIGRAPHY

Barrel Sheets

Information from macroscopic and microscopic examination of each core section was recorded by hand on a visual core-description (VCD) form. This information was condensed and entered into the AppleCORE (v8.1b) program to generate simplified graphic “barrel sheets” (see the “Core Descriptions” contents list). Site, hole, and mbsf interval are given at the top of the barrel sheet, with mbsf positions of core sections along the left margin. Copies of the original VCD sheets, which may contain additional core description, are available from ODP by request. Barrel sheet columns are discussed below, followed by an outline of the lithostratigraphic classification used for Leg 189.

Graphic Descriptions

The key for lithologic and contact symbols is presented in Figure F3. Lithologic symbols are arranged within the barrel sheet lithologic column in order of their relative abundance from left to right: minor lithologic modifiers (10%–25% in smear slide) are represented by 20%, major lithologic modifiers (>25%–50% in smear slide) by 30%, and the primary lithology by the remaining 50%–100%. If two minor modifiers are present, each is represented by 10% within the lithologic column, and if two major modifiers are present, each is represented by 15%. Lithologic contacts ranged from gradational (hashed thick line) to sharp (solid thin line).

Keys for sedimentary structures, lithologic accessories, ichnofossils, and fossils are presented in Figure F3. Isolated occurrences of these features are represented by a single symbol, whereas multiple to continuous occurrences are indicated by a vertical line with a centered symbol.

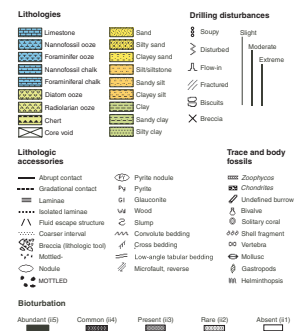
Bioturbation

Visible bioturbation was classified into five intensity levels based on the degree of disturbance of the physical sedimentary structures (Fig. F3):

1. Absent: No bioturbation; all physical sedimentary structures are preserved.
2. Rare: Isolated trace fossils; up to 10% of physical sedimentary structures are disrupted.
3. Present: ~10%–40% disrupted physical sedimentary structures; burrows are generally isolated but locally overlap.
4. Common: ~40%–60% bioturbated; last vestiges of physical sedimentary structures only are discernible.
5. Abundant: Bedding completely disturbed; burrows are still discrete in places.

These categories are based on the five ichnofossil indices (ii1–ii5) of Droser and Bottjer (1986). Visual recognition of bioturbation was often limited in homogeneous sediments, particularly white oozes; X-radiographic examination is warranted for such sediments.

F3. Key to symbols used in the barrel sheets, p. 40.



Drilling Disturbance

Drilling disturbance of relatively soft sediments (i.e., wherein intergrain motion was possible) was classified into five categories:

1. Slightly disturbed: Bedding contacts are slightly bent.
2. Moderately disturbed: Bedding contacts are extremely bowed.
3. Very disturbed: Bedding is completely deformed and may show diapiric or minor flow structures.
4. Flow-in: Sediments are completely disturbed with pervasive flow structures.
5. Soupy: Sediments are water saturated and show no traces of original bedding or structure.

To aid in evaluation of physical properties and other data, flow-in disturbance for each core beginning with Hole 1170A was rated on a qualitative scale as follows:

- F0 = undisturbed sediments with only minor "edge effect."
F1 = upward bowing of about one-third core width (~2.2 cm vertical stretching) or 30° inclination of sediments.
F2 = extreme upward bowing of about one-third to one-half core width (~2.2–3.4 cm vertical stretching) or 30°–60° inclination.
F3 = onset of minor flow-in beyond that of F2.
F4 = massive flow-in.

Drilling disturbance of lithified sediments (i.e., wherein intergrain motion was not likely because of compaction, cementation, etc.) was classified into three categories:

1. Fractured: Core pieces are in situ or partly displaced, but original orientation is preserved or recognizable; pieces may be supported by drill slurry or breccia.
2. Biscuit: Core pieces are from the cored interval and probably in correct stratigraphic sequence (although they may not represent the entire section), but original orientation is lost. Pieces are supported in drill mud.
3. Breccia: Core pieces have completely lost their original orientation and stratigraphic position.

To aid in evaluation of physical properties and other data, a qualitative disturbance rating was developed for biscuit and fractured lithified sediments to distinguish the amount of undisturbed "coherent" sediment from intercalated drill slurry and breccia, beginning with Hole 1170A. For each core section, the percentage of biscuits along the core center was estimated and rated as follows:

- B0 = >98% of undisturbed sediment.
B1 = 97%–91% of undisturbed sediment.
B2 = 90%–85% of undisturbed sediment.
B3 = 84%–70% of undisturbed sediment.
B4 = <70% of undisturbed sediment.

Samples

The positions of core samples are indicated in the sample column as follows: SS (smear slide), IW (interstitial water), PAL (micropaleontology), XRD (X-ray diffraction analysis), and TS (thin section). Contextual information includes sample location, whether the smear-slide or thin-section sample represents a dominant (D) or minor (M) lithology, and the estimated percentages of different grains.

Color

Reflectance of visible light was measured at 2-cm intervals for all core material using a Minolta Spectrophotometer (Model CM-2002) mounted on the archive multisensor track (AMST). The spectrophotometer was calibrated to zero once per shift. Regardless of sediment condition, archive-core measurements were made after the surface was saturated with water and covered with Gladwrap brand clear plastic wrap. This procedure protected the spectrophotometer lens and minimized variance caused by the degree of sediment wetness.

The measured visible light spectra provided a high-resolution stratigraphic record of color variations from 31 separate determinations of reflectance in 10-nm-wide spectral bands from 400 to 700 nm. These high-resolution data as well as high-precision Munsell color values measured at the same time are archived in the Janus database. Note that the precision of these values should not be confused with their accuracy in capturing stratigraphic patterns; core disturbances, particularly biscuiting and flow-in, require that such data be carefully evaluated against core photos and disturbance descriptions. Only major Munsell color changes, as determined by eye, using color charts, are reported in the barrel sheets. Additional information about measurement and interpretation of spectral data with the Minolta spectrophotometer can be found in Balsam et al. (1997, 1998, 1999).

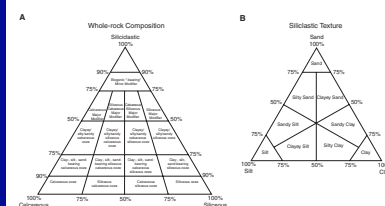
Description

The lithologic descriptions list the major lithology in capital letters, followed by descriptions of major and minor lithologies, and, finally, a description of other significant core features and their locations.

Lithologic Classification

The lithologic classification scheme for Leg 189 is based on three end-member components (i.e., biogenic siliceous, biogenic calcareous, and terrigenous siliciclastic), the texture of siliciclastics (i.e., clay-, silt-, sand-sized grains), and the degree of sediment induration (Fig. F4). Percentages of the different lithologic components, as well as siliciclastic textural percentages, were determined by smear-slide examination. These percentages defined the preliminary lithologies presented on the accompanying barrel sheets. Typically, smear slide-based estimates of percent carbonate often differed somewhat from subsequent coulometric-based measurements of percent carbonate. Where this carbonate offset produced different classifications for the major lithologic units within site summaries, the coulometric-based classification was preferred. Note that barrel sheet lithologies are based exclusively on smear slides and core observations available at the time of description and do not include coulometric results. Each compositional end-member of

F4. Whole-rock composition and siliciclastic classification schemes, p. 41.



the lithologic classification scheme is discussed in detail below and related graphically to one another in Figure F4.

Calcareous Biogenic

Calcareous biogenic lithologies are composed of >50% biogenous grains of which >50% are calcareous (Fig. F4A). Major (>25%–50%) and minor (10%–25%) modifiers describe the nature of the calcareous biogenic grains, as well as the composition of accessory siliceous biogenic or siliciclastic grains. Calcareous biogenic grains are described by the terms “foraminifer,” “nannofossil,” and “calcareous” (for unidentifiable grains), followed by the suffix “-bearing” where the component is present in minor amounts.

If the sediment was soft (i.e., readily deformed under the pressure of a finger or spatula blade and cut by the wire cutter), it was termed an ooze. If the sediment was firm (i.e., easily scratched by fingernail or edge of a spatula and cut by band or diamond saw), the term ooze was replaced by the term chalk. If the sediment was hard (i.e., not scratched by fingernail or edge of a spatula and cut by band or diamond saw), the term ooze was replaced by the term limestone. Additional modifiers for the texture of terrigenous sediments and the composition of accessory siliceous biogenic sediments were described using terms from the sections below (see “**Siliceous Biogenic**,” p. 8, and “**Siliciclastic Sediments**,” p. 9). For example, a firm sediment composed of 5% foraminifers, 15% siliciclastic silt, 18% diatoms, and 60% nannofossils would be termed a silt- and diatom-bearing nannofossil chalk. Note that multiple minor or major modifiers are listed in order of increasing predominance.

Siliceous Biogenic

Siliceous biogenic sediments are composed of >50% biogenous grains of which >50% are siliceous (Fig. F4A). Major and minor modifiers describe the composition of the siliceous biogenic grains, as well as the composition of accessory carbonate biogenic and siliciclastic grains. The composition of siliceous biogenic grains is described based on their origin using the terms “radiolarian,” “diatom,” “silicoflagellate,” and “siliceous” (for unidentifiable siliceous biogenic debris), followed by the suffix “-bearing” when a component is present in minor amounts. If the sediment was soft (i.e., readily deformed under the pressure of a finger or spatula blade and cut by the wire cutter), it was termed an ooze. If the sediment was firm (i.e., easily scratched by fingernail or edge of a spatula and cut by band or diamond saw), the term ooze was replaced by the term chalk. If the sediment was hard (i.e., not scratched by fingernail or edge of a spatula and cut by band or diamond saw), the term ooze was replaced by the term diatomite or radiolamite, as appropriate. Modifiers for the texture of siliciclastic sediments are described using terms from “**Siliciclastic Sediments**,” p. 9; the composition of accessory calcareous biogenic sediments is described using terms from “**Calcareous Biogenic**,” p. 8. For example, a soft sediment composed of 8% siliciclastic clay, 20% nannofossils, 35% radiolarians, and 37% diatoms would be termed a nannofossil-bearing radiolarian diatom ooze.

Siliciclastic Sediments

Siliciclastic sediments are composed of >50% siliciclastic grains and are classified according to the grain-size textures of clay (<3.9 μm), silt (3.9–6.25 μm), and sand (>6.25 μm –2.0 mm). The percentages of these three grain-size textures defined the major lithology based on the right ternary diagram in Figure F4B. Where the sediment was indurated (i.e., not easily scratched by fingernail or spatula edge), the suffix “-stone” was added (e.g., claystone, siltstone, and sandstone).

The predominant components of siliciclastic grains are described by major modifier terms such as “sand,” “silt,” or “clay” where any terms account for >25% of the siliciclastic percentage. Where biogenic grains are present in minor amounts (10%–25%) within siliciclastic it is followed by the suffix “-bearing.” Where a biogenic grain comprises >25%–50% of the total sediment, the major modifier of “siliceous” or “calcareous” (or more precise terms such as “radiolarian,” “foraminifer,” etc.; see above) is applied.

Three examples are presented to illustrate this siliciclastic classification. A sediment composed of 15% foraminifers, 25% glauconite, and 60% sand would be termed a foraminifer-bearing glauconitic sand. A sediment composed of 65% gravel and 35% silt would be termed a silty gravel. A sediment composed of 20% volcanic ash, 30% silt, and 50% sand would be termed an ash-bearing silty sand.

Clay Mineralogy

The purpose of this study was to recognize the major variations that occurred in the paleoenvironments, as expressed by the changing nature and abundance of clay minerals, using a sampling interval of one sample every two cores.

Methodology

The samples were decalcified using 10% acetic acid, then washed repeatedly with deionized water in a centrifuge. The carbonate-free fraction was deflocculated with a 1% Calgon (sodium hexametaphosphate) solution and homogenized in a sonic dismembrator for 1 min. The clay fraction (<2 μm) was separated by centrifugation, and the clay residue was then deposited onto glass slides and dried in an oven. Three separate X-ray analyses were run on each of the samples at a scan speed of 1° 2 θ /min using CuK α radiation, a Ni filter, and a monochromator. These were (1) from 2° to 32° 2 θ on a glass slide; (2) from 2° to 16° 2 θ on a slide saturated with ethylene glycol for 12 hr in an oven; and (3) on a slide heated to 550°C for 1 hr. Percentage evaluations calculated using MacDiff software were based on peak areas. The clay-mineral indexes smectite/smectite+illite (S/S+I), kaolinite/kaolinite+illite (K/K+I), and kaolinite/kaolinite+smectite (K/K+S) were derived from the ratios of the 001 smectite, illite, and kaolinite peak intensities obtained from the glycolated samples.

BIOSTRATIGRAPHY

Calcareous nannofossils, planktonic foraminifers, diatoms, palynomorphs (notably dinocysts), and radiolarians were the main groups examined and used for biostratigraphic zonation. Benthic foraminifers

and bolboformids were used to estimate paleobathymetry. Paleoenvironmental analysis was based on the integrated results of all microfossil groups. The abundance, preservation, and biostratigraphic assignment were entered into the Janus database (see the “[Related Leg Data](#)” contents list).

Preliminary ages were assigned based mainly on core-catcher samples. Additional samples (toothpick) were examined for nannofossils routinely. Where necessary to refine an age determination, additional samples from within the cores were also utilized.

The geochronologic scale for the various bioevents and epoch boundaries used is based on the geomagnetic polarity scheme as integrated by Berggren et al. (1995a, 1995b).

Calcareous Nannofossils

For Cenozoic sediments from Leg 189, the zonal schemes of Martini (1971) and Okada and Bukry (1980) were employed with some modifications. Previous southwest Pacific studies have shown these standard zonations are not always applicable in higher latitudes because of the absence or rarity of index species (Edwards and Perch-Nielsen, 1975). The main bioevents used are given in Table T1.

Nannofossil bioevents used in this study have been tentatively tied to the geochronologic scale of Berggren et al. (1995a, 1995b). Biomagnetostratigraphic correlations at several Southern Hemisphere high-latitude sites have shown considerably different ages (Wei and Wise, 1992) relative to those compiled from the mid-latitudes by Berggren et al. (1995a, 1995b). Correlation with shipboard magnetostratigraphy was essential for constraint of the nannofossil bioevents.

Methods

Smear slides were prepared for calcareous nannofossil study using standard techniques. Slides were examined using the light microscope under cross-polarized light, transmitted light, and phase-contrast light at 1000–1200× magnification. Relative abundance of each nannofossil species, overall preservation of the nannofossil assemblage, and the relative abundance of nannofossils were recorded for each sample. Taxonomic concepts follow those of Perch-Nielsen (1985) unless otherwise noted.

Preservation and abundance of calcareous nannofossil species varied significantly because of etching, dissolution, or calcite overgrowth. Preservation of assemblages was ranked according to the following criteria:

- VG=very good (no evidence of dissolution and/or overgrowth was found; no alteration of primary morphological characteristics were present; specimens were identifiable to the species level).
- G =good (little or no evidence of dissolution and/or overgrowth was found; primary morphological characteristics were only slightly altered; specimens were identifiable to the species level).
- M =moderate (specimens exhibit some etching and/or overgrowth; primary morphological characteristics were sometimes altered; however, most specimens were identifiable to the species level).
- P =poor (specimens are severely etched or exhibit overgrowth; primary morphological characteristics were largely destroyed;

T1. Ages of calcareous nannofossil bioevents, p. 50.

fragmentation had occurred; specimens could not be identified at the species and/or generic level).

Six calcareous nannofossil abundance levels for species and assemblages were recorded as follows in number of specimens per field of view:

- V = very abundant (11–100).
- A = abundant (1–10).
- C = common (1 per 2–10).
- F = Few (1 per 11–100).
- R = rare (1 per 101–1000).
- B = barren.

Planktonic and Benthic Foraminifers and Bolboformids

Zonation

The planktonic foraminiferal cool-subtropical (temperate) biostratigraphic scheme of Jenkins (1985, 1993a, 1993b), the Antarctic schemes of Stott and Kennett (1990) and Berggren et al. (1995b) formed the basis for the zonation used during Leg 189. The main bioevents (and others used during this leg) on which this scheme is based are given in Table T2. The geochronologic scale to which these bioevents are tied is that of Berggren et al. (1995a, 1995b).

Planktonic foraminiferal bioevents used in this study have been tentatively tied to the geochronologic scale (Fig. F5) of Berggren et al. (1995a, 1995b).

Benthic foraminifers provide only limited biostratigraphic age control, but they are useful in paleobathymetric and paleoenvironmental determinations. Interpretations in bathyal and abyssal depths, however, are difficult to standardize because the faunas are not strictly limited to specific water depths, but rather are a function of a large number of interrelated factors of which the supply of organic carbon and bottom-water oxygen content are considered most important. During Leg 189, use was made of guidelines for benthic foraminiferal depth distribution according to van Morkhoven et al. (1986) and Tjalsma and Lohmann (1983).

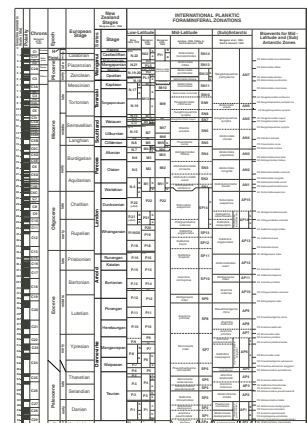
Bolboforma is an extinct group of spherical (70–250 µm in diameter) calcareous plankton that lived in temperate to cold waters of northern and southern middle to high latitudes. The group is tentatively placed in the Class Chrysophyceae (Tappan, 1980) with ~100 described species ranging from early Eocene to late Pliocene in age. The studies of Spiegler (1991) on Leg 114 material from the South Atlantic Ocean, Mackensen and Spiegler (1992) on Leg 120 material from the Kerguelen Plateau and Southern Indian Ocean, Kennett and Kennett (1990) on the Weddell Sea, Antarctica, and Spiegler (1999) on Leg 162 material from the North Atlantic Ocean suggest that the biostratigraphic utility of this group is high.

Sample Preparation

Most samples were prepared by soaking in a 10% hydrogen peroxide solution with Calgon for a short period and then washed over a 63-µm sieve. Harder samples were boiled for some time. All samples were washed with alcohol and then dried in an oven. Benthic foraminifers

T2. Ages of planktonic foraminiferal bioevents, p. 51.

F5. Planktonic foraminiferal bioevents and zonal schemes, p. 42.



were analyzed from the >125- μm -size fraction and, in only a few exceptions, from the >63- μm -size fraction.

Abundance and Preservation

For estimates of species abundance the following scale was used:

- P = present.
- T = trace (1–2 tests on tray).
- R = rare (3–5 tests on tray).
- F = frequent (6–14 tests on tray).
- C = common (>14 tests on tray).

The preservational state is described as follows:

- G = good (little or no fragmentation).
- M = moderate (some signs of fragmentation or alteration).
- P = poor (severe fragmentation or alteration).

Paleodepth

The depth-zonation scheme used is based on van Morkhoven et al. (1986), with the exception of the uppermost zone, which was redefined as follows:

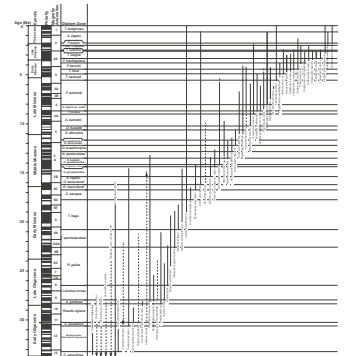
- Neritic to upper bathyal = 0–200 m.
- Upper bathyal = >200–600 m.
- Middle bathyal = >600–1000 m.
- Lower bathyal = >1000–2000 m.
- Upper abyssal = >2000–3000 m.
- Lower abyssal = >3000 m.

Diatoms

Diatom zonation for Leg 189 is based upon several zonal schemes developed for the southern high latitudes by Gersonde and Burckle (1990), Baldauf and Barron (1991), Harwood and Maruyama (1992), Gersonde and Bárcena (1998), and combined by Gersonde et al. (1998). Effectively, the scheme used during Leg 177 (Shipboard Scientific Party, 1999b), including their slight changes, was adopted for continuity in this work (Fig. F6). For instance the *Thalassiosira insigna*-*Thalassiosira vulnifica* Zone of Harwood and Maruyama (1992) is replaced by the *T. insigna* Zone (Shipboard Scientific Party, 1999b). This change was made because of the probable diachroneity of the first occurrence of *T. vulnifica*. It was also adopted during Leg 181 (Shipboard Scientific Party, 1999a) and was retained for Leg 189. In addition, the basal age of the *Fragilariopsis reinholdii* Zone, defined by the first occurrence (FO) of the nominate taxon, is placed at ~8.1 Ma within Chron C4 in accordance with Legs 177 and 181. This datum is close to that of the equatorial Pacific zonation (Barron, 1992). In addition to southern high-latitude diatoms, warm and temperate species were also encountered during Leg 189. Therefore, additional stratigraphic ranges have been added following the compilation of Barron (1992).

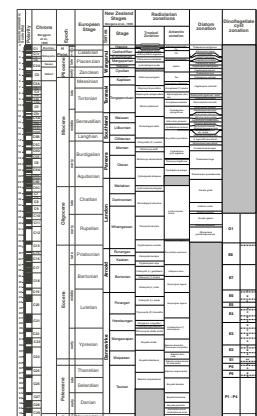
Age assignments for the zones used are listed in Table T3. The zonation is tied to the geomagnetic polarity time scale of Berggren et al. (1995a, 1995b) and is presented with species ranges in Figure F7.

F6. Diatom species ranges, p. 43.



T3. Ages of diatom bioevents, p. 52.

F7. Tentative correlation between the siliceous microplankton and dinoflagellate zonal schemes and geochronologic scale, p. 44.



Methods

Two methods of diatom analysis were followed. For assessment of the overall abundance of the group, smear slides were prepared from a small amount of core-catcher material or from additional core material. For intervals rich in carbonate, as much as 10 cm³ of raw sample was treated with 35% HCl. For organic-rich intervals, samples were treated with up to 30% H₂O₂ before carbonate removal. Residues were washed with distilled water several times to remove the acid. For both methods, permanent slides were made by mounting the sediment on glass slides protected by a glass cover slip using Hyrax or Norland Optical Adhesive mounting media. All slides were examined in their entirety for stratigraphic markers and paleoenvironmentally sensitive taxa using a Zeiss compound microscope at 400× magnification. Identifications were confirmed when necessary at 1000× magnification. The counting method of Schrader and Gersonde (1978) was adopted. Photomicrographs of poorly known taxa were made using a video-print system at 1500× final magnification.

Overall diatom abundance was determined from smear-slide analysis at 400× magnification according to the following convention in values per traverse of cover slip:

- A = abundant (>150).
- C = common (>80–150).
- F = few (>30–80).
- R = rare (5–30).
- T = trace (<5).
- B = barren (no diatoms observed).

Species relative abundance was determined with the following convention in percent of assemblage:

- D = dominant (>50%).
- A = abundant (>30%–50%).
- C = common (>15%–30%).
- F = few (3%–15%).
- R = rare (<3%).
- T = trace (occasional occurrence).
- P = present (applicable to diatoms where diatom valves could not be counted individually [e.g., *Ethmodiscus rex* fragments], or for all taxa with trace/rare overall abundance).

Preservation of diatoms was determined qualitatively according to the following convention:

- G = good (finely silicified forms present and no alteration [dissolution or fragmentation] of valves).
- M = moderate (finely silicified forms present, but some alteration of valves).
- P = poor (finely silicified forms rare or absent, valves fragmented, and assemblage dominated by heavily silicified forms).

Radiolarians

Zonation

No useful radiolarian zones for temperate regions of the Southern Hemisphere have been published. This study temporarily utilizes Antarctic and subtropical zonal schemes. Antarctic zones have been compiled from Abelmann (1990, 1992), Caulet (1991), Chen (1975), Hollis (1993, 1997), Lazarus (1992), Nishimura (1987), Takemura (1992), and Takemura and Ling (1997), and tropical zones are modified from Sanfilippo and Nigrini (1998).

The main bioevents (and others used during this leg) on which this scheme is based are given in Table T4. Radiolarian bioevents used in this study have been tentatively tied to the geochronologic scale (Fig. F7) of Berggren et al. (1995a, 1995b).

T4. Ages of radiolarian bioevents, p. 53.

Sample Preparation

Radiolarians were extracted using standard leaching techniques. Most samples were disaggregated by boiling in a solution of 10% H₂O₂ and 5% HCl. After rinsing the disaggregated sediment through a 63- μ m sieve, the residues were placed in an oven at 60°C for a minimum of 1 hr. As a final process, the residues were uniformly distributed on glass slides using Norland Optical Adhesive mounting media.

Abundance and Preservation

Several hundred species were encountered under the microscopic observations of 100 \times to 400 \times magnifications. For age determination, only age-diagnostic radiolarian taxa were identified. Overall, radiolarian abundance was determined by strewn-slide evaluation of 100 specimens, using the following conventions:

- C = common (>50 specimens per slide traverse).
- F = few (10–50 specimens per slide traverse).
- R = rare (<10 specimens per slide traverse).
- T = trace (1 or a few specimens are encountered in one overall slide).
- B = barren (no radiolarians in sample).

The relative abundance of individual species was recorded as follows:

- A = abundant (>10% of the total assemblage).
- C = common (>5%–10% of the total assemblage).
- F = few (1%–5% of the total assemblage).
- R = rare (<1% of the total assemblage).
- T = trace (1 to 3 specimens per slide).

The state of preservation was determined using the following criteria:

- VG=very good (nearly pristine, complete skeleton, lacking any indication of dissolution, recrystallization, or breakage).
- G =good (majority of specimens complete; minor dissolution, recrystallization, and/or breakage).
- M =moderate (minor but common dissolution; small amount of recrystallization or breakage of specimens).

P = poor (strong dissolution, recrystallization, or breakage; many specimens unidentifiable).

Palynology, Dinoflagellate Cysts

Zonation

No integrated, calibrated dinoflagellate cyst (dinocyst) Cenozoic zonal schemes have been established for the Southern Ocean. In effect, little is known of Neogene organic walled dinocysts from the Southern Ocean. For the Paleogene, use will be made of the combined regional schemes and/or bioevents from Australia (e.g., Partridge, *op. cit.*, Truswell, 1997) and New Zealand (e.g., Wilson, 1984, 1988; Raine et al., 1997). In addition, available data of the Tertiary from the Southern Ocean region will be taken into account (e.g., Goodman and Ford, 1983; Wrenn and Hart, 1988; Wilson, 1989; Mohr, 1990; Mao and Mohr, 1995, among others). Encountered dinocyst events will be compared with these previous investigations, and with the succession of events and zones established by Bujak and Mudge (1994), Bujak and Brinkhuis (1998), and Williams et al. (1998a) for the Northern Hemisphere Cenozoic to allow cross-hemisphere correlations and assessment of paleoprovincialism.

Initial stratigraphic assessment of occurring Paleogene terrestrial palynomorphs are made using the schemes of Truswell (1997) and MacPhail (1999).

Processing

Up to 10 cm³ of sample was processed according to standard palynological treatment. Briefly, the procedure includes digestion by HCl and HF, followed by HCl leaching, and centrifuging after each step. Residues were sieved using a stainless steel 20- μ m sieve and strew-mounted on slides using glycerine jelly. In some cases, heavy-liquid separation using a ZnCl₂ solution is applied (in quartz-rich sediments). A minimum of two slides were prepared and counted for a minimum of 150 specimens.

Abundance, Preservation, and Taxonomy

For indications of group abundance, the following scale is used:

B = barren.
T = trace.
F = few.
C = common.
A = abundant.

When possible, counts of >100 palynomorphs (broad categories) and, subsequently, >200 dinocysts were made.

Preservation is classified as one of the following:

P = poor.
M = moderate.
G = good.

Taxonomy is in accordance with that cited in Williams et al. (1998b).

Sediment Accumulation Rates

We used an estimation of sedimentation rates determined by age vs. depth data for each site. Ages follow the geochronological scale outlined in “[Biostratigraphy](#),” p. 9. Paleomagnetic data for each site were calibrated to the calcareous microfossil biostratigraphic events. A table of the bioevents used for the age-depth plots is included with each site chapter.

Biostratigraphic data were used as a first estimate of the age of the sediments at each site, from the time scale used in this volume. This permitted the correlation of the paleomagnetic data to the published paleomagnetic time scale, which yielded age determinations that were used to adjust the age estimates for the stratigraphic section.

Periods of continuous sedimentation on the age-depth curves are indicated by solid lines, and hiatuses are denoted by dashed lines. Average rates of sedimentation during each epoch are given within each figure.

PALEOMAGNETISM

Paleomagnetic and rock magnetic investigations aboard the *JOIDES Resolution* during Leg 189 included routine measurements of natural remanent magnetizations (NRM). Initially archive-half sections were used, but later whole cores were used. Both were measured before and after alternating-field (AF) demagnetization to 20 mT. Low-field magnetic susceptibility (k) measurements were made with the MST. NRMs and a limited set of rock magnetic observations were made with discrete samples. A nonmagnetic APC core barrel assembly was used for alternate cores in selected holes and the magnetic overprints in core recovered with this assembly were compared with those obtained with standard assemblies.

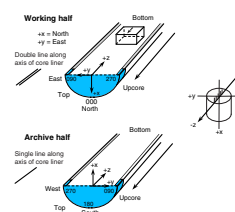
Measurement Procedure

The remanence measurements made during Leg 189 were conducted using the shipboard pass-through cryogenic magnetometer. The standard ODP magnetic coordinate system was used (+x = vertical upward from the split surface of archive halves, +y = left along split surface when looking upcore, and +z = downcore; see Fig. F8).

The output of the 2G magnetometer is given in magnetic moment in electromagnetic units with a background noise of $\sim 10^{-7}$ Gauss cm (SI $\times 10^{-10}$ A/m²). This gives an approximate limit in intensity of magnetization required for reliable measurements of standard half- or whole-core samples, reaching the order of 10^{-6} A/m, or 0.001 mA/m. However, it should be noted that the magnetization of core liners can exceed this intensity. For standard discrete samples, the weakest measurable intensity is more than an order of magnitude greater than the long cores because of the smaller volume of material in the pickup coils.

Natural remanent magnetization was initially measured on all archive-half sections. However, after comparisons between half-core and whole-core measurements revealed that core splitting sometimes induced significant overprints, whole cores were measured for the remainder of the leg. Core flow through the laboratory was modified with the long-core measurement being made before the MST run, which sped up processing significantly.

F8. Magnetic orientation convention, p. 45.



Long-core measurements were made at 5-cm intervals with 15-cm-long headers and trailers. Measurements at core and section ends and within intervals of drilling-related core deformation were removed during data processing. AF demagnetizations were applied to cores at 20 mT, and when time permitted, a 10-mT step was also measured.

Discrete samples were collected from the working halves in standard 8-cm³ plastic cubes using the extrusion tool. The discrete samples were analyzed on the shipboard pass-through cryogenic magnetometer using a tray designed for measuring six discrete samples. To maintain the ODP convention, the cube face with the arrow on it is placed downward in the tray. Samples were demagnetized by AF using the in-line demagnetizer installed on the pass-through cryogenic magnetometer. They were given anhysteretic and isothermal remanent magnetizations (ARM and IRM), and these were demagnetized to establish the magnetic characteristics of the recovered core. Magnetic susceptibility was measured for each whole-core section as part of the MST analysis (see “[Physical Properties](#),” p. 22). Susceptibility is measured on the MST using a Bartington MS2 meter coupled to a MS2C sensor coil with a diameter of 88 cm operating at 0.565 kHz. The sensor was set on SI units, and the data were stored in the Janus database in raw meter units. The sensor coil is sensitive over an interval of ~4 cm (half-power width of the response curve), and the width of the sensing region corresponds to a volume of 166 cm³ of cored material. To convert to true SI volume susceptibilities, these values should be multiplied by 10⁻⁵ and then multiplied by a correction factor to take into account the volume of material that passed through the susceptibility coils. Except for measurements near the end of each section, the correction factor for a standard full ODP core is about 0.66 (= 1/1.5). The end effect of each core section was not corrected.

Core Orientation

During APC coring, full orientation was achieved with the Tensor multishot tool rigidly mounted onto a nonmagnetic sinker bar. The Tensor tool consists of three mutually perpendicular magnetic field sensors and two perpendicular gravity sensors. The information from both sets of sensors allows the azimuth and dip of the hole to be measured as well as the azimuth of the APC core double orientation line.

Magnetostratigraphy

Where magnetic cleaning successfully isolated the characteristic remanent magnetization (ChRM), paleomagnetic inclinations were used to define magnetic polarity zones. On some occasions, it was possible to recover a satisfactory magnetic stratigraphy even when the inclination was of a single polarity because of a persistent overprint. On such occasions, there were indications of the magnetic stratigraphy in the intensity and associated minor differences in the inclination (Fig. F8). To recover the magnetostratigraphy, the z-component alone was used. The z-component was biased in one direction but showed a clear alternating signal superposed upon this. By removing the bias, the magnetization with alternating sign, which carries the magnetostratigraphic signal, is made clearer. Interpretations of the magnetic polarity stratigraphy, with constraints from the biostratigraphic data, are presented in each of the site chapters. The revised time scale of Cande and Kent (1995), as pre-

sented in Berggren et al. (1995a, 1995b), was used as a reference for the ages of Cenozoic polarity chrons.

COMPOSITE DEPTHS

The recovery of complete sediment sections over APC-cored intervals was crucial to the paleoceanographic objectives of Leg 189. Drilling of multiple holes at each site ensured that intervals missing from one APC hole as a result of recovery gaps between cores were recovered in an adjacent hole. During Leg 189, as on previous ODP legs, continuity of recovery was confirmed by composite depth sections developed for all multiple cored sites. The methods used during Leg 189 were similar to those used to construct composite depth sections during Leg 138 (Hagelberg et al., 1992), Leg 154 (Curry, Shackleton, Richter, et al., 1995), Leg 162 (Jansen, Raymo, Blum, et al., 1996), and Leg 167 (Lyle, Koizumi, Richter, et al., 1997).

At each site, closely spaced (2- to 4-cm interval) measurements of magnetic susceptibility and gamma-ray attenuation (GRA) bulk density were made on the MST soon after the core sections had equilibrated to room temperature. These measurements were entered into the shipboard database and minimally processed. In addition, measurements of spectral reflectance were made at 2-cm resolution on the split cores (see “[Lithostratigraphy](#),” p. 5). Magnetic susceptibility, lightness (L^*) values from the spectral reflectance measurements, and GRA bulk density measurements from each hole were compared to determine if coring offsets were maintained between holes. Integration of at least two different physical properties allowed hole-to-hole correlations to be made with greater confidence than would be possible with only a single data set.

Hole-to-hole correlations were made using interactive software developed specifically for this task. We used a software package for Unix platforms that was developed by the Borehole Research Group at LDEO and was patterned after the Leg 138 correlation software. Corresponding features in data sets from adjacent holes were aligned based on graphical and mathematical cross-correlations by using an iterative process. Features were aligned by adjusting the ODP coring depths in mbsf, measured from the length of the drill string advanced, on a core-by-core basis. No depth adjustments were made within a core. The resulting adjusted depth scale is the meters composite depth (mcd) scale.

The composite depth section for each site is presented in tabular form in the “Composite Depths” section of each site chapter. The composite depth table of Site 1171 is given as an example in Table T5. For each core, the depth adjustment required to convert from the mbsf depth scale to the mcd scale is given. The last two columns in each table give, for each core, the cumulative-depth offset added to the ODP curatorial sub-bottom depth (in mbsf) and the composite depth (in mcd), respectively. The depth-offset column facilitates conversion of sample depths that are recorded in ODP curatorial sub-bottom depth (in mbsf) to composite depth (in mcd). The equivalent depth in mcd is obtained by adding the amount of offset listed to the depth in mbsf of a sample taken in a particular core.

Adjustments to the shipboard mbsf depth scale are required for several reasons (see the short summaries in Ruddiman et al., 1987; Farrell and Janecek, 1991; Hagelberg et al., 1992; and Hagelberg et al., 1995). Rebound of the sediment following core recovery causes the cored sedi-

T5. Composite depth section,
p. 54.

ment sequence to be expanded relative to the drilled interval. In addition, other factors including random variations in ship motion and heave can affect the true in situ depth of each core by introducing errors. Even between successive cores having nominally 100%, or even greater, recovery, portions of the sediment sequence are usually missing. As a result, the composite depth scale grows downhole relative to the mbsf scale, typically on the order of 10%.

The need for a composite section to verify stratigraphic continuity is illustrated in Figure F9. In the leftmost panel, GRA bulk density from three holes at Site 1171 is shown on the mbsf depth scale. In the middle panel, the same records are shown after depth scale adjustment so that correlative features are aligned.

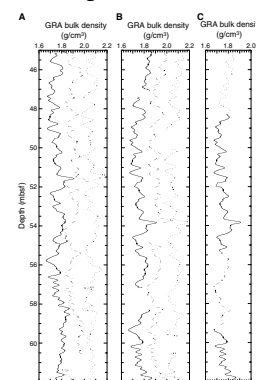
The correlation of lithologic parameters between multiple holes and associated depth adjustments for individual cores was optimized in such a way that a single record could be sampled from the aligned cores without any additional depth scale changes. Where the amount of offset necessary to align features was ambiguous or imprecise for all lithologic parameters or where multiple hole data were unavailable, no additional depth adjustments were made. In these cases, the total amount of offset between mbsf depth and mcd is equal to the cumulative offset from the overlying cores. The composite depth section extends only to the base of multiple cored intervals, typically the APC intervals at Sites 1168–1172. Below the multiple cored intervals, cores were appended using the offset of the last core within the composite record to convert mbsf to mcd.

For each site, after the composite section was constructed, a representative record was assembled. Because the missing intervals between successive cores in the sedimentary sequence could be identified, it was possible to patch in these missing intervals with data from adjacent holes. The resulting splice provides a single representative record of each lithologic parameter (i.e., susceptibility, spectral reflectance, and GRA bulk density) for a given site. Additionally, these single records are ideally suited to serving as sampling schemes for paleoceanographic studies.

Splice tie points were made between adjacent holes at identifiable, highly correlated features. Each splice was constructed by beginning at the mudline at the top of the composite section and working downward. Typically, one hole is chosen as the backbone for the record and cores from other holes are used to patch in the missing intervals in the core gaps (Fig. F9). Intervals were chosen for the splice such that section continuity was maintained, whereas disturbed intervals were avoided. An example of a table that provides tie points for the Site 1171 splice is given in Table T6. Tables that give the tie points for construction of the spliced records are presented in each site chapter (Tables T15, p. 153, in the “Site 1168” chapter, T16, p. 149, in the “Site 1170” chapter, T16, p. 158, in the “Site 1171” chapter, T15, p. 133, in the “Site 1172” chapter).

By identifying intervals where features present in the multiple holes were most highly correlated, it was possible to construct a spliced record that avoided duplication or omission of any individual features or cycles. Splice tie points always connect features with exactly the same composite depths. As a result, the final alignment of the adjacent holes could be slightly different from the one giving the best overall visual or quantitative hole-to-hole correlation. Further adjustments to the composite depth section by expanding and compressing the depth scale within individual core intervals would be required to align all fea-

F9. Portions of the GRA bulk density records, p. 46.



T6. Splice tie points, p. 55.

tures exactly. These additional adjustments will be made as part of normal postcruise studies.

ORGANIC GEOCHEMISTRY

The shipboard organic geochemistry program for Leg 189 included three routine sets of analyses. First, headspace (and vacutainer where appropriate) analysis for volatile hydrocarbons (and other gases) were performed as required by ODP safety regulations. Second, elemental analyses of total carbon, total nitrogen, and total sulfur content of sediment samples (and calculation of total organic carbon) were determined. Third, organic matter type and maturity was characterized using C/N ratios and Rock-Eval pyrolysis. Most of the procedures and instruments used during Leg 189 are described by Emeis and Kvenvolden (1986) and generally are the same as those used during most recent ODP legs. Brief comments on routine sampling and deviations from standard practice are noted below; more detailed notes are presented in the "Explanatory Notes" chapters of ODP *Initial Reports* Volumes 150, 156, 164, and 181 (Shipboard Scientific Party, 1994, 1995, 1996, 1998).

Volatile Hydrocarbons and Other Gases

Sediment gas composition was determined at least once from every core. The primary sampling technique was headspace sampling. For the headspace method, a cork borer was used to obtain a measured volume of sediment from the top of one section of each core immediately after on-deck retrieval. The sediment, with a typical volume of ~5 cm³, was placed in a 21.5-cm³ glass serum vial that was sealed with a septum and metal crimp cap. When consolidated or lithified samples were encountered, rock chips were placed in the vial and sealed. Before gas analysis, the vial was heated at 60°C for 30 min. A 5-cm³ volume of the headspace gas was extracted from each vial using a standard glass syringe. Gaseous voids visible through the core liner were sampled using a syringe and vacutainer.

Two gas chromatography (GC) systems were used for gas analysis: a Hewlett-Packard 5890 Series II GC and a Hewlett-Packard 5890A natural gas analyzer. The Series II GC determines concentration of C₁ (methane), C₂ (ethane), and C₃ (propane) hydrocarbons with a flame ionization detector (FID). The natural gas analyzer measures concentrations of C₁ through C₇ hydrocarbons with an FID as well as N₂, O₂, and CO₂ with a thermal conductivity detector (TCD). For both systems, the chromatographic response was calibrated to standard gas mixtures.

Total Organic Carbon Content and Elemental Analyses

Total carbon, nitrogen, and sulfur contents of sediment samples were determined with a Carlo Erba Model NA1500 CNS analyzer. Approximately 6 mg of freeze-dried, ground sediment was combusted in oxygen at 1000°C. In this process, helium acts as a carrier gas, the oxygen is removed, and the combustion gases are reduced and separated by GC and quantified with a TCD. Total organic carbon (TOC) content was calculated as the difference between total carbon (TC) and the inorganic (carbonate) carbon (IC) value generated by carbonate coulometry (i.e., TOC = TC - IC).

Organic Matter Characterization

The origin of sedimentary organic matter can be characterized using organic carbon/nitrogen (C/N) values generated by the CNS analyzer. The average C/N ratio of marine zoo- and phytoplankton is between 5 and 8, whereas terrestrially derived organic matter has ratios between 25 and 35 (e.g., Emerson and Hedges, 1988; Meyers, 1994).

Sedimentary organic matter type and quality were further evaluated by Rock-Eval pyrolysis of hydrocarbons (Espitalié et al., 1986). In this procedure, volatile hydrocarbon content (in milligrams per gram of sample) released by heating at 300°C for 3 min is measured by the FID and labeled as an S₁ peak on the Rock-Eval pyrogram. Hydrocarbon quantity (in milligrams of hydrocarbon per gram of sediment) produced by pyrolysis as the temperature is increased from 300° to 600°C at a heating rate of 25°C/min is also measured by the FID and is called the S₂ peak. The nominal temperature at which the maximum rate of hydrocarbon yield is attained during S₂ analysis is the T_{max} value, which roughly equates to thermal maturity. CO₂ (in milligrams per gram), generated between 300° and 390°C, is measured using a TCD and is called the S₃ peak. TOC is calculated from S₁, S₂, and S₃ and from the oxidation of the remaining carbon in the sediment sample measured by a second TCD. The carbon-normalized hydrogen index (HI) (in milligrams of hydrocarbon per gram of carbon) and oxygen index (OI) (in milligrams of carbon dioxide per gram of carbon) are calculated from pyrolysis values by $HI = (100 \times S_2)/TOC$, and $OI = (100 \times S_3)/TOC$.

INORGANIC GEOCHEMISTRY

Shipboard interstitial water (IW) analyses for Leg 189 were conducted on 5- to 15-cm-long whole-round sediment sections cut and capped immediately after the core arrived on deck. The general sampling frequency utilized the following scheme: three samples per core in the upper ~60–70 mbsf, followed by one per core from 60 to 100 mbsf, then one every third core to total depth. Before squeezing, the outer rind of each whole-round sediment section was carefully scraped with a stainless steel spatula to remove potential contamination.

Interstitial waters were extracted by placing the whole-round samples in a titanium and stainless steel squeezing device that is a modified version of the standard stainless steel squeezer of Manheim and Sayles (1974). Squeezing was performed at ambient temperature by applying as much as 40,000 lb of pressure (~4150 psi) with a Carver laboratory hydraulic press (Model 2702). Interstitial water was extruded first through a prewashed Whatman No. 1 filter and then through a 0.45-µm Gelman polysulfone disposable filter into a precleaned plastic syringe. After collecting up to 30 mL of interstitial water, the syringe was removed to dispense aliquots for shipboard and shore-based analyses.

Interstitial water analyses followed the procedures outlined by Gieskes et al. (1991). Salinity as total dissolved solids was routinely measured with a Goldberg optical handheld Reichart refractometer. Alkalinity was measured immediately after squeezing by Gran titration with a Brinkmann pH electrode and a Metrohm autotitrator; pH was determined on the National Bureau of Standards scale as part of the alkalinity titration. Dissolved chloride (Cl⁻) was determined by titration with AgNO₃. Dissolved silica (H₄SiO₄⁰) and ammonium (NH₄⁺) concen-

trations were measured using a Milton Roy Spectronic 301 spectrophotometer. Standard seawater from the International Association for the Physical Sciences of the Ocean was used for calibrating most techniques.

Calcium, magnesium, potassium, and sulfate were determined on 1/200 diluted aliquots in nanopure water using a Dionex DX-120 ion chromatograph. Lithium and strontium concentrations were quantified by inductively coupled plasma-atomic emission spectroscopy (ICP-AES) with a Jobin Yvon JY2000. Tenfold dilutions of the interstitial water were used for all ICP elemental studies. Standards for all ICP-AES techniques were initially matrix matched as closely as possible to samples using filtered surface seawater spiked with the appropriate concentrations of specific elements and serially diluted according to the method outlined by Murray et al. (2000). However, we noticed that the Ba²⁺ spike to the standard solutions resulted in precipitation of barite (BaSO₄), leading to poor Ba reproducibility. In addition, during subsequent tests with SO₄²⁻-free synthetic seawater solutions, we also noticed that we could not reproduce Sr²⁺ concentrations measured during initial runs using surface seawater. We inferred that Sr²⁺ was being coprecipitated with the barite in the standards, resulting in anomalously high Sr²⁺ concentrations in unknowns. Therefore, we began reanalysis of samples for Sr²⁺ concentrations using the standards matrix matched with synthetic seawater, which resulted in similar trends but with reduced and more realistic absolute values. Only Sr²⁺ data obtained with the synthetic seawater standards are reported. Because we could not further test possible SO₄²⁻-free solution matrix effects, the Sr²⁺ data should be viewed with caution, although trends are probably real. No effect on Li⁺ values was observed between surface seawater and synthetic seawater standards, which are considered robust. The precision of the methods based on replicate analyses are reported in Table T7.

PHYSICAL PROPERTIES

Introduction

The primary goals of physical properties measurements during Leg 189 were to (1) calibrate the near-continuous records of physical properties that were used for hole-to-hole correlations, construction of complete stratigraphic sequences, and core-to-downhole log ties; (2) examine gradients in physical properties, such as porosity, natural gamma radiation, magnetic susceptibility, and compressional wave velocity, which are related to variations in sediment composition; and (3) provide data to aid the interpretation of seismic reflection and downhole geophysical logs. Initial measurements of physical properties are undertaken on the MST. These measurements are performed on unsplit, 1.5-m-long (and shorter) sections and are nondestructive. The MST incorporates a GRA bulk density device, a *P*-wave logger (PWL), a magnetic susceptibility meter (MSM), and a natural gamma sensor (NGR). The quality of the MST data is highly dependent upon the condition of the core. Bulk density and magnetic susceptibility measurements were taken at 2-cm intervals on the MST. The PWL measurements were taken at 2-cm intervals in APC cores only. Natural gamma data were not routinely measured. Thermal conductivity, using the needle-probe method, was also measured at discrete intervals in whole-round sections. Physical properties measurements made on split-core sections in-

T7. Relative standard deviations for analysis of dissolved species, p. 56.

cluded undrained shear strength, and longitudinal, transverse, and orthogonal compressional wave velocity. Moisture and density (MAD) measurements determined for discrete samples included dry bulk density, grain density, porosity, and void ratio. One MAD sample per section was taken in the Pleistocene and Pliocene sections of the A holes; three samples per core were taken in Miocene through Paleogene sections.

Multisensor Track

The GRA bulk density device allows an estimation of wet bulk density by measuring the attenuation of gamma rays passing through the cores, where the degree of attenuation is proportional to density (Boyce, 1976; Gerland and Villinger, 1995; Breitzke, 2000). Calibration of the system was conducted using a known seawater/aluminum density standard with four components of different average densities.

The PWL transmits a 500-kHz compressional wave pulse through the core at 1 kHz. The transmitting and receiving transducers are aligned perpendicular to the core axis. A pair of displacement transducers monitors the separation between the compressional wave transducers so that the variations in the outside diameter of the liner do not degrade the accuracy of the velocities. Where there is poor acoustic coupling between the sediment and the liner, the PWL does not provide accurate velocity values and therefore is used only on undisturbed APC cores. Calibration of the displacement transducer and measurement of electronic delay within the PWL circuitry were conducted using a series of acrylic blocks of known thickness and *P*-wave traveltime. Calibration validity was checked by measuring the *P*-wave velocity through a section filled with distilled water.

Whole-core magnetic susceptibility was measured at 2-cm intervals on a Bartington MS2C meter with an 80-mm (internal diameter) loop sensor using a 1-s integration time and averaging five readings. Susceptibility values were archived in raw instrument units (SI), which require multiplication by 6.6×10^{-6} to convert to volume-normalized SI units. The accuracy of the GRA, PWL, and MSM measurements are degraded in APC and XCB sections with gas voids, where the core does not fill the liner completely, or is disturbed. Nevertheless, in such cases the downhole trends are still useful for stratigraphic correlation.

Natural gamma-ray emission was not routinely measured because of time constraints imposed by the high recovery rate. NGR data were recorded on selected holes, mainly at 10- to 20-cm intervals along each section. The area of influence for the four NGR sensors is about 10 cm from each point of measurement along the core axis. The installation and operating principles of the NGR system used on the *JOIDES Resolution* are discussed by Hoppie et al. (1994). Data from 2048 energy channels were collected and archived. Counts were summed over the range from 200 to 3000 keV (in five windows), so as to be comparable with data collected during previous legs. This integration range also allows for a direct comparison with downhole logging data, which are collected over a similar integration range (Hoppie et al., 1994). Over the 200- to 3000-keV integration range, background counts (measured using a core liner filled with distilled water) averaged 18 per 30 s measurement period. No corrections were made to XCB core NGR data to account for inaccuracies resulting from core liners that were incompletely filled with sediment. Before taking measurements, the four sensor gains were adjusted so that the combined potassium peak was as sharp as the

individual peaks when the other three were disabled. The multichannel analyzer was then calibrated by assigning certain channels to the characteristic energies of ^{40}K and the main peak of ^{232}Th (Blum, 1997).

Spectrophotometry

The archive MST (AMST 188 version) was used to make systematic measurements of the relative spectral reflectance of the sediment surfaces. The instrument consists of a computer-controlled motorized track assembly that advances a set of detectors over the cut sediment surface of a core half. The sensors include an LB1101 laser displacement transducer measuring the sediment micromorphology and a Minolta CM-2002 spectral photometer. The laser displacement transducer was run before every scan to obtain information on the drop-down distance for the spectrophotometer. The controller software allows manual configuration and calibration for all sensors and automatically runs scans of core sections.

The Minolta CM-2002 spectrophotometer uses a pulsed xenon arc lightbulb, which illuminates a round aperture 0.8 cm in diameter. The light reflection is focused on a silicon photodiode and measures the wavelength range between 400 and 700 nm (in 10-nm steps) and the $L^* a^* b^*$ (lightness, red/green, and yellow/blue chromaticity coordinate) values. These data are also converted into the Munsell color scheme. The Minolta CM-2002 spectrophotometer was calibrated every 24 hr by a zero-measurement (aperture open to infinity) and a white calibration using the standard white ceramic lid supplied by Minolta. Measurements were taken at 2-cm intervals on all APC, XCB, and RCB cores at each site. The Minolta CM-2002 spectrophotometer is designed to operate in direct contact with the sediment surface, and the offset was set to -0.1 units in relation to the laser-measured distance. In order to protect the aperture, the sediment was covered with Gladwrap brand clear plastic wrap. Dried sediment sections were moistened with distilled water.

Moisture and Density Measurements

Samples of $\sim 10\text{ cm}^3$ were taken from the fresh core for determination of moisture and density (MAD) measurements. Bulk density, grain density, water content, porosity, and dry density were calculated from wet and dry sample weights and dry volumes. Sample mass was determined with an error within 0.1% using a Scitech electronic balance. The balance was equipped with a computer averaging system that corrected for ship accelerations. The sample mass was counterbalanced by a known mass such that the mass differentials generally were $<1\text{ g}$. Sample volumes were determined using a Quantachrome Penta-Pycnometer, a helium-displacement pycnometer with a precision of $\pm 0.04\text{ cm}^3$. Sample volumes were determined at least three times, until the last two measurements had $<0.01\%$ standard deviation. A standard reference volume was run with each group of samples during the measurements and rotated among the cells to check for instrument drift and systematic error. A purge time of 3 min was used before each run. The sample beakers used for discrete determinations of moisture and density were calibrated before the cruise. Dry weight and volume measurements were performed after the samples were oven dried at $105^\circ \pm 5^\circ\text{C}$ for 24 hr and allowed to cool in a desiccator. Water content, bulk density, porosity, grain density, dry density, and void ratio were determined following the procedures and equations outlined in Blum (1997). The procedures for

the determination of these properties comply with the American Society for Testing and Materials (ASTM) designation (D) 2216 (ASTM, 1990).

Velocimetry

In addition to the velocity measurements with the PWL, compressional wave velocity was measured on split-core sections with the digital sound velocimeter (PSW1 and PSW2) using two types of piezoelectric transducer pairs. The transducers were inserted into soft sediments along (z-direction) and orthogonal (y-direction) to the core axis. Velocity calculation is based on the fixed distance between the transducers (7 and 3.5 cm, respectively), measurement of the traveltime of an acoustic impulse, and a delay constant determined by measuring a water standard. Periodically, the separation was precisely evaluated by running a calibration procedure in distilled water. A value of the sound velocity in distilled water is determined (based on standard equations) for the measured temperature, with the computer calculating the transducer separation using the signal traveltime. Use of the PSW1 and PSW2 was stopped in more indurated sediments when the sediment started to crack during insertion of the transducers. The modified Hamilton frame velocimeter was also used, which measured the traveltime of a 500-kHz signal orthogonally across the split-core section and core liner (x-direction). Orientation of the x-, y-, and z-directions is indicated in Shipboard Scientific Party (1997; fig. 12). Sample thickness was measured directly from the velocimeter frame lead screw through a linear resistor output to a digital multimeter. Zero traveltimes for the velocity transducers were estimated by a linear regression of traveltime vs. distance for a series of aluminum and lucite standards. Velocity data recorded in the Janus database are uncorrected for in situ temperature and pressure. However, these corrections can be made using the relationships in Wylie et al. (1956), Wilson (1960), and Mackenzie (1981).

Undrained Shear Strength

The undrained shear strength (S_u) of the sediment was determined using the ODP motorized miniature vane shear device following the procedures of Boyce (1977). The vane rotation rate was set to 90°/min. Measurements were made only in the fine-grained, soft to very stiff units. A range of springs of various strengths were available; the B-4 spring was used during this leg. The spring was calibrated before the start of the leg. The instrument measures the torque and strain at the vane shaft using a torque transducer and potentiometer, respectively. The shear strength reported is the peak strength determined from the torque vs. strain plot. In addition to the peak shear strength, the residual strength was determined from the same plot where the failure was not dominated by cracking of the sample (Pyle, 1984). In the analysis of vane tests, the assumption is made that a cylinder of sediment is uniformly sheared around the axis of the vane in an undrained condition, with cohesion as the principal contributor to shear strength. Departures from this assumption include progressive cracking within and outside the failing specimen, uplift of the failing core cylinder, drainage of local pore pressures (i.e., the test can no longer be considered to be undrained), and stick-slip behavior.

Thermal Conductivity

The TK04 (Teka Bolin) was used for thermal conductivity measurements. The full-space needle probe, containing a heater wire and a calibrated thermistor, was inserted into the unconsolidated sediment through a small hole drilled into the core liner. Three measuring cycles were automatically performed at each location. At the beginning of each test, a self-test, which included a drift study, was conducted. Once the samples were equilibrated, the heater circuit was closed and the temperature rise in the probes was recorded. Thermal conductivities were calculated from the rate of temperature rise while the heater current was flowing. Temperatures measured during the first 150 s of the heating cycle were fitted to an approximate solution of a constantly heated line source (for details see Kristiansen, 1982, and Blum, 1997). Errors are between 5% and 10%. Corrections were not attempted for in situ temperature or pressure effects.

In Situ Temperature Measurements

In situ temperature measurements were made with the Adara tool and the Davis Villinger Temperature Probe (DVTP). The Adara tool is housed entirely inside the coring shoe of the APC. In a normal deployment, the tool first stops briefly at the mudline before entering the borehole and thermally equilibrates with the bottom water. After the APC penetrates to the bottom sediments, it is held there for ~10 min and records the temperature of the cutting shoe every 5 s. As a result of the frictional heating caused by the APC penetration, the temperature rises instantaneously but decreases gradually as the heat dissipates to the surrounding sediments. One can theoretically extrapolate the equilibrium temperature of the sediment by applying a mathematical heat conduction model to the temperature decay record (Horai and Von Herzen, 1985). More technical instrument information can be found in *Initial Reports* Volumes 139 and 150 (Shipboard Scientific Party, 1992, 1994).

In a normal deployment in deep water (>2000 m), the mudline stop can be very short (<5 min) because the thermal gradient of the bottom water is near zero and the APC is already approaching thermal equilibrium during the long descent. The time between the surface deployment and the mudline stop is very short. In addition, the water circulated within the drill pipe can be several degrees warmer than the ambient bottom water, although the circulation pump is usually shut off just before the mudline stop. Therefore, it takes ~10 min before the APC shoe thermally equilibrates with the bottom water at the mudline.

The DVTP tool is used in semilithified sediments, which the APC cannot penetrate, and unlike the Adara, the DVTP requires a separate wireline run. This tool measures formation temperature using a probe that is pushed into the top of the sediment section. The probe is conical with two thermistors, one located 1 cm from the tip of the probe and the other 12 cm above the tip. A third thermistor, referred to as the internal thermistor, is located in the electronics package. Thermistor sensitivity is 1 mK in an operating range from -5° to 20°C , and the total operating range is -5° to 100°C . The thermistors were calibrated at the factory and on the laboratory bench before installation in the probe. In addition to the thermistors, the probe contains an accelerometer sensitive to 0.98 m/s^2 . Both peak and mean acceleration are recorded by the logger. The accelerometer data are used to track disturbances to the in-

strument package during the equilibration interval. In a DVTP deployment, mudline temperatures are measured for 10 min on the first run within each hole and for 2 min for subsequent runs before descent into the hole for a 10-min equilibration interval in the bottom. Mudline temperatures are also collected for at least 2 min on ascent. Data from the probe tip thermistor are used for estimation of in situ temperatures.

Data reduction procedures are similar for both temperature tools. The synthetic thermal decay curves for the Adara tool and DVTP are a function of the geometry and thermal properties of the probe and the sediments (Bullard, 1954; Horai and von Herzen, 1985). However, it is never possible to obtain a perfect match between the synthetic curves and the data because (1) the probe never reaches thermal equilibrium during the penetration period; (2) contrary to theory, the frictional pulse upon insertion is never instantaneous; and (3) temperature data are sampled at discrete intervals, meaning that the exact time of penetration is always uncertain. Thus, both the effective penetration time and equilibrium temperature must be estimated by applying a fitting procedure, which involves shifting the synthetic curves in time to obtain a match with the recorded data. The data collected >20–50 s after penetration usually provide a reliable estimate of equilibrium temperature. However, where the APC has not achieved a full stroke, leakage of drilling fluid into the formation may occur and results are not considered reliable.

DOWNHOLE MEASUREMENTS

Introduction

Well logging provides continuous in situ records of geophysical parameters within a borehole. These measurements are used to assess the physical, chemical, and structural characteristics of formations penetrated by drilling and, thus, provide a means of reconstructing and interpreting geologic environments.

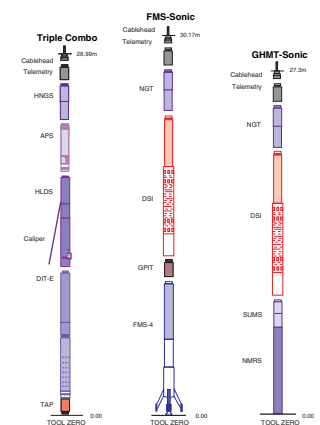
Well logging is typically undertaken in the deepest hole drilled at any one site. Where core recovery is poor, downhole logs are often the most reliable source of information; where core recovery is good, log data can be correlated with core data to produce more detailed results.

Downhole logging operations begin after the hole has been cored and flushed with a viscous drilling fluid. The drilling assembly is then pulled up to ~80 mbsf and the logging tools are passed through the drill pipe into the open hole. The logging tools are joined together into tool strings so that compatible tools are run together. Each tool string is lowered separately to the base of the hole, and then measurement takes place as the tool string is raised at a constant velocity between 275 and 500 m/hr (see individual site chapters). A wireline heave compensator is used to minimize the effect of the ship's heave on the tool position in the borehole (Goldberg, 1990).

Tool-String Configurations

Three tool strings were used during Leg 189: the triple combination (triple combo), the Formation MicroScanner-sonic (FMS-sonic) string, and the geologic high-resolution magnetic tool (GHMT) string (Fig. F10; Tables T8, T9). The principles underlying the use of these tools are explained on the LDEO Borehole Research Group's Web site (see the

F10. Wireline tool strings used during Leg 189, p. 47.



T8. Wireline tool strings used and properties measured, p. 57.

T9. Acronyms used for the wireline tool strings and their measurements, p. 58.

“Related Leg Data” contents list) and in Schlumberger (1989), Serra (1984, 1986, 1989), Timur and Toksöz (1985), and Tittman (1986). Some examples of the logging tools’ applications are given by Ellis (1987) and Rider (1996). The following is a more concise description and explanation of the tools used.

Natural Gamma-Ray Sonde and the Hostile-Environment Natural Gamma-Ray Sonde

The natural gamma-ray sonde (NGS) and the hostile-environment natural gamma-ray sonde (HNGS) measure the gamma radiation of uranium, potassium, and thorium, which occur naturally in sediments. Because of the relative abundance of U, Th, and K within many clay minerals, a high gamma-ray reading is often indicative of a relatively high clay content in the sediment, whereas a low gamma-ray reading often indicates quartz sands and carbonates (e.g., Serra and Sulpice, 1975). It should be mentioned, however, that this is not always the case (see Rider, 1990).

A gamma-ray sonde was fitted to all of the tool strings to enable depth correlation between each individual logging run. The data from the HNGS on the triple-combo are used as the reference gamma log because the HNGS produces a more precise measurement than the NGS (Schlumberger, 1994). The natural gamma reading was also used for measuring the depth to the seafloor, as natural gamma radiation shows a sharp increase at the mudline.

Accelerator Porosity Sonde

The accelerator porosity sonde (APS) emits fast neutrons, which lose energy as they collide with hydrogen nuclei in the formation. Once the neutrons have slowed down to reach thermal energies (0.025 eV), they are captured by the nuclei of chlorine and various heavy elements. This results in a gamma-ray emission. The APS measures the number of neutrons arriving at five different detectors at varying distances from the source. This measurement is inversely proportional to the concentration of hydrogen in the formation. Because the majority of hydrogen is contained in the pore water, the APS measurement can be used to derive a porosity. However, hydrogen bound in minerals, such as clays, also contributes to the APS measurement, so that the raw porosity value is often an overestimate. Furthermore, the presence of certain rare earth and trace elements with particularly large capture cross sections (e.g., boron and cadmium) can have a significant effect on the APS reading (Harvey et al., 1996).

Hostile-Environment Lithodensity Sonde

The hostile-environment lithodensity sonde (HLDS) consists of a ^{137}Cs radioactive source and two gamma-ray detectors mounted on a shielded sidewall skid that is pressed against the formation by a hydraulically activated arm. This arm also provides a caliper measurement of borehole diameter. The gamma rays emitted by the source interact with the electrons in the formation and lose energy as a result of Compton scattering. When gamma-ray energy is low (<150 keV), photoelectric absorption takes place. This tool is sensitive to hole conditions, as the

detectors need to be in contact with the borehole wall to produce reliable data.

The number of gamma rays that reach the detectors in the HLDS is directly related to the number of electrons in the formation, which is in turn related to the bulk density. The bulk density value measured by the HLDS can be used to calculate a porosity, using the following equation:

$$\Phi = (\rho_{gr} - \rho_b) / (\rho_{gr} - \rho_w),$$

where ρ_{gr} = mean grain density, given by physical properties measurements (typically 2.7 g/cm³), ρ_w = pore-water density, taken to be 1.03 g/cm³ for seawater, and ρ_b = bulk density, given by the HLDS.

The photoelectric effect (PEF) can be assessed by comparing the counts from the far detector of the HLDS, which is in the high-energy region where only Compton scattering occurs, with those of the near detector, which is in the low-energy region where the PEF is dominant. Photoelectric absorption is strongly dependent on the atomic number of the constituents of the formation. The PEF values, therefore, can give an indication of the chemical composition of the rock.

Dual Induction Tool

The dual induction tool (DIT) provides three different measurements of electrical resistivity based on multiple depths of investigation: deep induction (IDPH), medium induction (IMPH), and shallow, spherically focused resistivity (SFL). The two induction devices produce an alternating magnetic field, which induces Foucault currents around the borehole. These currents produce a new inductive signal, proportional to the conductivity of the formation. The measured conductivities are then converted to resistivity (in ohm-meters). The SFL measures the current necessary to maintain a constant voltage drop across a fixed interval and is a direct measurement of resistivity. Because the solid constituents of rocks are essentially infinitely resistive relative to the pore fluids, resistivity is controlled mainly by the nature of the pore fluids, porosity, and the permeability.

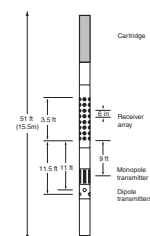
Temperature/Acceleration/Pressure Tool

The temperature/acceleration/pressure (TAP) tool uses both fast- and slow-response thermistors to detect borehole fluid temperature at two different rates. The fast-response thermistor is able to detect small abrupt changes in temperature, whereas the slow-response thermistor is used to estimate temperature gradient and thermal regimes more accurately. Data from the TAP tool provide an insight into the thermal regime of the formation penetrated by drilling. A three-axis accelerometer is also used to measure tool movement downhole, which allows the effects of heave to be analyzed.

Dipole Shear Sonic Imager

The dipole shear sonic imager (DSI) employs a combination of monopole and dipole transducers (see Fig. F11) to make accurate measurements of sonic wave propagation in a wide variety of lithologies (Schlumberger, 1995). In addition to robust and high-quality determination of compressional wave velocity, the DSI excites a flexural mode in the borehole that can be used to determine shear-wave velocity in all

F11. The dipole shear sonic imager, p. 48.



types of formations. When the formation shear velocity is less than the borehole fluid velocity, particularly in unconsolidated sediments, the flexural wave travels at shear-wave velocity and is the most reliable means to estimate a shear velocity log. The configuration of the DSI also allows recording of cross-line dipole waveforms. These modes can be used to estimate shear-wave splitting caused by preferred mineral and/or structural orientations in consolidated formations. A low-frequency source enables Stoneley waveforms to be acquired as well.

General Purpose Inclinometry Tool

The general purpose inclinometry tool (GPIT) uses acceleration measurements to calculate the amount of tool displacement that occurs during logging. The GPIT contains a triple-axis accelerometer and a triple-axis magnetometer. The GPIT records the orientation of the FMS images and allows more precise determination of log depths than can be determined from cable length, which may experience stretching and/or be affected by ship heave.

Formation MicroScanner

The FMS produces high-resolution microresistivity images. This tool consists of four orthogonal imaging pads, each containing 16 microelectrodes (Fig. F12). The pads, which are in direct contact with the borehole wall, emit a focused current into the formation. The current intensity fluctuations are measured, then converted to color images that reflect microresistivity variations: the lighter the color, the greater the resistivity (Ekstrom et al., 1987). These images have a vertical resolution of ~0.5 cm and a measurement interval of 0.25 cm (Serra, 1989). Roughly 30% of a 25-cm-diameter borehole is imaged.

The development of the FMS tool has added a new dimension to wireline logging (Luthi, 1990; Lovell et al., 1998; Salimullah and Stow, 1992). The formation can now be viewed in its complete state, and often it can be grouped into facies assemblages. Features such as bedding, fracturing, slump folding, and bioturbation can be resolved, and the fact that the images are oriented means that fabric can be analyzed and bed orientations measured.

Susceptibility Magnetic Sonde

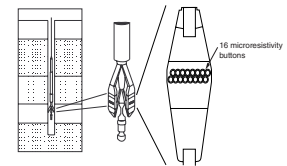
The susceptibility magnetic sonde (SUMS) measures magnetic susceptibility by means of low-frequency induction in the surrounding sediment. Magnetic susceptibility responds primarily to magnetic minerals (mainly magnetite, hematite, and iron sulfide), which are often contained in the detrital sediment fraction and, therefore, can be used as a proxy indicator of paleoenvironmental change.

Nuclear Magnetic Resonance Sonde

The nuclear magnetic resonance sonde (NMRS) measures the total magnetic field using a proton precession magnetometer. The data from the SUMS and the NMRS tools can be used to construct a polarity stratigraphy using the method outlined below.

The total magnetic field (B) measured in the borehole is composed of five variables:

F12. Schematic diagram of the Formation MicroScanner, p. 49.



$$B = B_o + B_p + B_t + B_i \pm B_r,$$

where B_o is the Earth's magnetic field, generated in the Earth's core with an intensity of ~63,000 nT for the region of Leg 189; B_p is the magnetic field caused by the bottom-hole assembly (BHA) and pipe and can be up to ~2000 nT, decaying away from the BHA; B_t is the time varying field (Two passes of the GHMT are run to check that this is negligible. If only one pass of the GHMT is run, then B_t is assumed to be negligible); B_i is the field induced in the borehole by the effect of the Earth's field acting on the sediments (It is given by the formula $B_i = [(J_i/2) \cdot (1-3 \sin^2 I)]$, where $J_i = B_o \cdot c$. The sediment susceptibility, c , is measured by the SUMS, I is the magnetic inclination of the modern Earth's field [B_o] at the borehole location), and B_r is the remnant field in the borehole (In the Southern Hemisphere, negative B_r signifies a normal polarity whereas positive B_r signifies reversed polarity).

$B_i \pm B_r$ are the fields of interest. Subtracting the above-mentioned fields from that measured by the GHMT yields $B_i \pm B_r$. A stratigraphy based solely on positive or negative remanence is a reasonable estimate of the true magnetic stratigraphy. Further postcruise analysis will give a more reliable result.

REFERENCES

- Abelmann, A., 1990. Oligocene to middle Miocene radiolarian stratigraphy of southern high latitudes from Leg 113, Sites 689–690, Maud Rise. *In* Barker, P.F., Kennett, J.P., et al., *Proc. ODP, Sci. Results*, 113: College Station, TX (Ocean Drilling Program), 675–708.
- , 1992. Early to middle Miocene radiolarian stratigraphy of the Kerguelen Plateau, Leg 120. *In* Wise, S.W., Jr., Schlich, R., et al., *Proc. ODP, Sci. Results*, 120: College Station, TX (Ocean Drilling Program), 757–783.
- ASTM, 1990. Standard method for laboratory determination of water (moisture) content of soil and rock. *In* *Annual Book of ASTM Standards* (Vol. 04.08): Philadelphia (Am. Soc. Testing and Mater.), D 2216–90 (revision of 2216–63, 2216–80).
- Baldauf, J.G., and Barron, J.A., 1991. Diatom biostratigraphy: Kerguelen Plateau and Prydz Bay regions of the Southern Ocean. *In* Barron, J., Larsen, B., et al., *Proc. ODP, Sci. Results*, 119: College Station, TX (Ocean Drilling Program), 547–598.
- Balsam, W.L., Damuth, J.E., and Schneider, R.R., 1997. Comparison of shipboard vs. shore-based spectral data from Amazon Fan cores: implications for interpreting sediment composition. *In* Flood, R.D., Piper, D.J.W., Klaus, A., and Peterson, L.C. (Eds.), *Proc. ODP, Sci. Results*, 155: College Station, TX (Ocean Drilling Program), 193–215.
- Balsam, W.L., Deaton, B.C., and Damuth, J.E., 1998. The effects of water content on diffuse reflectance measurements of deep-sea core samples: An example from ODP Leg 164 sediments. *Mar. Geol.*, 149:177–189.
- , 1999. Evaluating optical lightness as a proxy for carbonate content in marine sediment cores. *Mar. Geol.*, 161:141–153.
- Barron, J.A., 1992. Neogene diatom datum levels in the equatorial and north Pacific. *In* Ishizaki, K., and Saito, T. (Eds.), *The Centenary of Japanese Micropaleontology*: Tokyo (Terra Sci. Publ.), 413–425.
- Berggren, W.A., Hilgen, F.J., Langereis, C.G., Kent, D.V., Obradovich, J.D., Raffi, I., Raymo, M.E., and Shackleton, N.J., 1995a. Late Neogene chronology: new perspectives in high-resolution stratigraphy. *Geol. Soc. Am. Bull.*, 107:1272–1287.
- Berggren, W.A., Kent, D.V., Swisher, C.C., III, and Aubry, M.-P., 1995b. A revised Cenozoic geochronology and chronostratigraphy. *In* Berggren, W.A., Kent, D.V., Aubry, M.-P., and Hardenbol, J. (Eds.), *Geochronology, Time Scales and Global Stratigraphic Correlation*. Spec. Publ.—Soc. Econ. Paleontol. Mineral. (Soc. Sediment. Geol.), 54:129–212.
- Blum, P., 1997. Physical properties handbook: a guide to the shipboard measurement of physical properties of deep-sea cores. *ODP Tech. Note*, 26 [Online]. Available from World Wide Web: <<http://www.odp.tamu.edu/publications/tnotes/tn26/INDEX.HTM>> [Cited 2001-01-03].
- Boyce, R.E., 1976. Definitions and laboratory techniques of compressional sound velocity parameters and wet-water content, wet-bulk density, and porosity parameters by gravimetric and gamma-ray attenuation techniques. *In* Schlanger, S.O., Jackson, E.D., et al., *Init. Repts. DSDP*, 33: Washington (U.S. Govt. Printing Office), 931–958.
- , 1977. Deep Sea Drilling Project procedures for shear strength measurement of clayey sediment using modified Wykeham Farrance laboratory vane apparatus. *In* Barker, P.F., Dalziel, I.W.D., et al., *Init. Repts. DSDP*, 36: Washington (U.S. Govt. Printing Office), 1059–1068.
- Breitzke, M., 2000. Physical properties of marine sediments. *In* Schulz, H.O., Zabel, M. (Eds.), *Marine Geochemistry*: Berlin (Springer Verlag).
- Bujak, J.P., and Brinkhuis, H., 1998. Global warming and dinocyst changes across the Paleocene/Eocene boundary. *In* Aubry, M.-P., et al. (Eds.), *Late Paleocene-Early Eocene Climatic and Biotic Events in the Marine and Terrestrial Records*: New York (Columbia Univ. Press), 277–295.

- Bujak, J.P., and Mudge, D.C., 1994. A high-resolution North Sea Eocene dinocyst zonation. *J. Geol. Soc. London*, 151:449–462.
- Bullard, E.C., 1954. The flow of heat through the floor of the Atlantic Ocean. *Proc. R. Soc. London A*, 222:408–429.
- Cande, S.C., and Kent, D.V., 1995. Revised calibration of the geomagnetic polarity timescale for the Late Cretaceous and Cenozoic. *J. Geophys. Res.*, 100:6093–6095.
- Caulet, J.-P., 1991. Radiolarians from the Kerguelen Plateau, Leg 119. In Barron, J., Larsen, B., et al., *Proc. ODP, Sci. Results*, 119: College Station, TX (Ocean Drilling Program), 513–546.
- Chen, P.-H., 1975. Antarctic radiolaria. In Hayes, D.E., Frakes, L.A., et al., *Init. Repts. DSDP*, 28: Washington (U.S. Govt. Printing Office), 437–513.
- Curry, W.B., Shackleton, N.J., Richter, C., et al., 1995. *Proc. ODP, Init. Repts.*, 154: College Station, TX (Ocean Drilling Program).
- Droser, M.L., and Bottjer, D.J., 1986. A semiquantitative field classification of ichnofabric. *J. Sediment. Petrol.*, 56:558–559.
- Edwards, A.R., and Perch-Nielsen, K., 1975. Calcareous nannofossils from the southern Southwest Pacific, DSDP Leg 29. In Kennett, J.P., Houtz, R.E., et al., *Init. Repts. DSDP*, 29: Washington (U.S. Govt. Printing Office), 469–539.
- Ekstrom, M.P., Dahan, C., Chen, M.-Y., Lloyd, P., and Rossi, D.J., 1987. Formation imaging with microelectrical scanning arrays. *Log Analyst*, 28:294–306.
- Ellis, D.V., 1987. *Well Logging for Earth Scientists*: New York (Elsevier).
- Emeis, K.-C., and Kvenvolden, K.A., 1986. Shipboard organic geochemistry on *JOIDES Resolution*. *ODP Tech. Note*, 7.
- Emerson, S., and Hedges, J.I., 1988. Processes controlling the organic carbon content of open ocean sediments. *Paleoceanography*, 3:621–634.
- Espitalié, J., Deroo, G., and Marquis, F., 1986. La pyrolyse Rock-Eval et ses applications, Partie III. *Rev. Inst. Fr. Pet.*, 41:73–89.
- Farrell, J.W., and Janecek, T.R., 1991. Late Neogene paleoceanography and paleoclimatology of the northeast Indian Ocean (Site 758). In Weissel, J., Peirce, J., Taylor, E., Alt, J., et al., *Proc. ODP, Sci. Results*, 121: College Station, TX (Ocean Drilling Program), 297–355.
- Gerland, S., and Villinger, H., 1995. Nondestructive density determination on marine sediment cores from gamma-ray attenuation measurements. *Geo-Mar. Lett.*, 15:111–118
- Gersonde, R., and Bárcena, M.A., 1998. Revision of the late Pliocene-Pleistocene diatom biostratigraphy for the northern belt of the Southern Ocean. *Micropaleontology*, 44:84–98.
- Gersonde, R., and Burckle, L.H., 1990. Neogene diatom biostratigraphy of ODP Leg 113, Weddell Sea (Antarctic Ocean). In Barker, P.F., Kennett, J.P., et al., *Proc. ODP, Sci. Results*, 113: College Station, TX (Ocean Drilling Program), 761–789.
- Gersonde, R., Spiess, V., Flores, J.A., Hagan, R., and Kuhn, G., 1998. The sediments of Gunnerus Ridge and Kainan Maru Seamount (Indian sector of the Southern Ocean). *Deep-Sea Res.*, 45:1515–1540.
- Gieskes, J.M., Gamo, T., and Brumsack, H., 1991. Chemical methods for interstitial water analysis aboard *JOIDES Resolution*. *ODP Tech. Note*, 15.
- Goldberg, D., 1990. Test performance of the Ocean Drilling Program wireline heave compensator. *Sci. Drilling*, 1:206–209.
- Goodman, D.K., and Ford, L.N., Jr., 1983. Preliminary dinoflagellate biostratigraphy for the middle Eocene to Lower Oligocene from the Southwest Atlantic Ocean. In Ludwig, W.J., Krasheninnikov, V.A., et al., *Init. Repts. DSDP*, 71: Washington (U.S. Govt. Printing Office), 859–977.
- Hagelberg, T., Shackleton, N., Pisias, N., and Shipboard Scientific Party, 1992. Development of composite depth sections for Sites 844 through 854. In Mayer, L., Pisias, N., Janecek, T., et al., *Proc. ODP, Init. Repts.*, 138 (Pt. 1): College Station, TX (Ocean Drilling Program), 79–85.

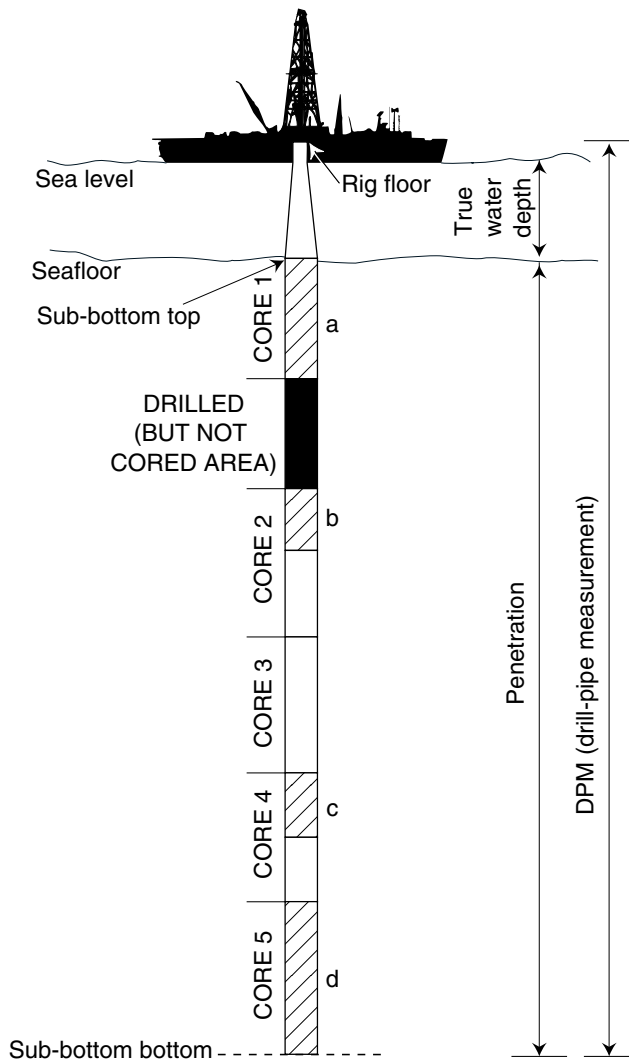
- Hagelberg, T.K., Pisias, N.G., Shackleton, N.J., Mix, A.C., and Harris, S., 1995. Refinement of a high-resolution, continuous sedimentary section for studying equatorial Pacific Ocean paleoceanography, Leg 138. In Pisias, N.G., Mayer, L.A., Janecek, T.R., Palmer-Julson, A., and van Andel, T.H. (Eds.), *Proc. ODP, Sci Results*, 138: College Station, TX (Ocean Drilling Program), 31–46.
- Harvey, P.K., Lovell, M.A., Brewer, T.S., Locke, J., and Mansley, E., 1996. Measurement of thermal neutron absorption cross section in selected geothermal reference materials. *Geostand. Newsl.*, 20:79–85.
- Harwood, D.M., and Maruyama, T., 1992. Middle Eocene to Pleistocene diatom biostratigraphy of Southern Ocean sediments from the Kerguelen Plateau, Leg 120. In Wise, S.W., Jr., Schlich, R., et al., *Proc. ODP, Sci. Results*, 120: College Station, TX (Ocean Drilling Program), 683–733.
- Hollis, C.J., 1993. Latest Cretaceous to Late Paleocene radiolarian biostratigraphy: a new zonation from the New Zealand region. *Mar. Micropaleontol.*, 21:295–327.
- , 1997. Cretaceous-Paleocene Radiolaria of eastern Marlborough, New Zealand. *Inst. Geol. Nucl. Sci. Monogr.*, 17.
- Hoppie, B.W., Blum, P., and the Shipboard Scientific Party, 1994. Natural gamma-ray measurements on ODP cores: introduction to procedures with examples from Leg 150. In Mountain, G.S., Miller, K.G., Blum, P., et al., *Proc. ODP, Init. Repts.*, 150: College Station, TX (Ocean Drilling Program), 51–59.
- Horai, K., and Von Herzen, R.P., 1985. Measurement of heat flow on Leg 86 of the Deep Sea Drilling Project. In Heath, G.R., Burckle, L.H., et al., *Init. Repts. DSDP*, 86: Washington (U.S. Govt. Printing Office), 759–777.
- Jansen, E., Raymo, M.E., Blum, P., et al., 1996. *Proc. ODP, Init. Repts.*, 162: College Station, TX (Ocean Drilling Program).
- Jenkins, D.G., 1985. Southern mid-latitude Paleocene to Holocene planktic foraminifera. In Bolli, H.M., Saunders, J.B., and Perch-Nielsen, K. (Eds.), *Plankton Stratigraphy*: Cambridge (Cambridge Univ. Press), 263–282.
- , 1993a. Cenozoic southern mid- and high-latitude biostratigraphy and chronostratigraphy based on planktonic foraminifera. In Kennett, J.P., and Warnke, D.A. (Eds.), *The Antarctic Paleoenvironment: A Perspective on Global Change*. *Antarct. Res. Ser.*, 60:125–144.
- , 1993b. The evolution of the Cenozoic Southern high- and mid-latitude planktonic foraminiferal faunas. *The Antarctic Paleoenvironment: a Perspective of Global Change*. *Antarct. Res. Ser.*, 60:175–194.
- Kennett, D.M., and Kennett, J.P., 1990. *Bolboforma* Daniels and Spiegler, from Eocene and lower Oligocene sediments, Maud Rise, Antarctica. In Barker, P.F., Kennett, J.P., et al., *Proc. ODP, Sci. Results*, 113: College Station, TX (Ocean Drilling Program), 667–673.
- Kristiansen, J.I., 1982. The transient cylindrical probe method for determination of thermal parameters of earth materials [Ph.D. dissert.]. Aarhus Univ.
- Lazarus, D., 1992. Antarctic Neogene radiolarians from the Kerguelen Plateau, Legs 119 and 120. In Wise, S.W., Jr., Schlich, R., et al., *Proc. ODP, Sci. Results*, 120: College Station, TX (Ocean Drilling Program), 785–809.
- Lovell, M.A., Harvey, P.K., Brewer, T.S., Williams, C., Jackson, P.D., and Williamson, G., 1998. Application of FMS images in the Ocean Drilling Program: an overview. In Cramp, A., MacLeod, C.J., Lee, S.V., and Jones, E.J.W. (Eds.), *Geological Evolution of Ocean Basins: Results from the Ocean Drilling Program*. *Geol. Soc. Spec. Publ. London*, 131:287–303.
- Luthi, S.M., 1990. Sedimentary structures of clastic rocks identified from electrical borehole images. In Hurst, A., Lovell, M.A., and Morton, A.C. (Eds.), *Geological Applications of Wireline Logs*. *Geol. Soc. Spec. Publ. London*, 48:3–10.
- Lyle, M., Koizumi, I., Richter, C., et al., 1997. *Proc. ODP, Init. Repts.*, 167: College Station, TX (Ocean Drilling Program).
- Mackensen, A., and Spiegler, D., 1992. Middle Eocene to early Pliocene *Bolboforma* (algae?) from the Kerguelen Plateau, southern Indian Ocean. In Wise, S.W., Jr.,


- Schlich, R., et al., *Proc. ODP, Sci. Results*, 120: College Station, TX (Ocean Drilling Program), 675–682.
- Mackenzie, K.V., 1981. Nine-term equation for sound speed in the oceans. *J. Acoust. Soc. Am.*, 70:807–812.
- MacPhail, M.K., 1999. Palynostratigraphy of the Murray Basin, inland southeastern Australia. *Palynology*, 23:197–240.
- Manheim, F.T., and Sayles, F.L., 1974. Composition and origin of interstitial waters of marine sediments, based on deep sea drill cores. In Goldberg, E.D. (Ed.), *The Sea* (Vol. 5): *Marine Chemistry: The Sedimentary Cycle*: New York (Wiley), 527–568.
- Mao, S., and Mohr, B.A.R., 1995. Middle Eocene dinoflagellate cysts from Bruce Bank (Scotia Sea, Antarctica) and their palaeoenvironmental and palaeogeographic conclusions. *Rev. Palaeobot. Palynol.*, 86:235–263.
- Martini, E., 1971. Standard Tertiary and Quaternary calcareous nannoplankton zonation. In Farinacci, A. (Ed.), *Proc. 2nd Int. Conf. Planktonic Microfossils Roma*: Rome (Ed. Tecnosci.), 2:739–785.
- Meyers, P.A., 1994. Preservation of elemental and isotopic source identification of sedimentary organic matter. *Chem. Geol.*, 144:289–302.
- Mohr, B.A.R., 1990. Eocene and Oligocene sporomorphs and dinoflagellate cysts from Leg 113 drill sites, Weddell Sea, Antarctica. In Barker, P.F., Kennett, J.P., et al., *Proc. ODP, Sci. Results*, 113: College Station, TX (Ocean Drilling Program), 595–612.
- Murray, R.W., Miller, D.J., and Kryc, K.A., 2000. Analysis of major and trace elements in rocks, sediments, and interstitial waters by inductively coupled plasma–atomic emission spectrometry (ICP-AES). *ODP Tech. Note*, 29 [Online]. Available from World Wide Web: <<http://www-odp.tamu.edu/publications/tnotes/tn29/INDEX.HTM>>. [Cited 2001-01-03] [N2].
- Nishimura, A., 1987. Cenozoic Radiolaria in the western North Atlantic, Site 603, Leg 93 of the Deep Sea Drilling Project. In van Hinte, J.E., Wise, S.W., Jr., et al., *Init. Repts. DSDP*, 93 (Pt. 2): Washington (U.S. Govt. Printing Office), 713–737.
- Okada, H., and Bukry, D., 1980. Supplementary modification and introduction of code numbers to the low-latitude coccolith biostratigraphic zonation (Bukry, 1973; 1975). *Mar. Micropaleontol.*, 5:321–325.
- Perch-Nielsen, K., 1985. Cenozoic calcareous nannofossils. In Bolli, H.M., Saunders, J.B., and Perch-Nielsen, K. (Eds.), *Plankton Stratigraphy*: Cambridge (Cambridge Univ. Press), 427–554.
- Pyle, M.R., 1984. Vane shear data on undrained residual strength. *J. Geotech. Engr. Div., Am. Soc. Civ. Eng.*, 110:543–547.
- Raine, J.I., Askin, R.A., Crouch, E.M., Hannah, M.J., Levy, R.H., and Wrenn, J.H., 1997. Palynomorphs. In Hannah, M.J., and Raine, J.I. (Eds), *Southern Ocean Late Cretaceous/Early Cenozoic Biostratigraphic Datums*. Inst. Geol. Nucl. Sci., Sci. Rept., 97:25–33.
- Rider, M., 1990. Gamma-ray log shape used as a facies indicator: critical analysis of an oversimplified method. In Hurst, A., Lovell, M.A., and Morton, A.C. (Eds.), *Geological Application of Wireline Logs*. Geol. Soc. Spec. Publ. London, 48:27–37.
- , 1996. *The Geological Interpretation of Well Logs* (2nd ed.): Caithness (Whittles Publishing).
- Ruddiman, W.F., Cameron, D., and Clement, B.M., 1987. Sediment disturbance and correlation of offset holes drilled with the hydraulic piston corer: Leg 94. In Ruddiman, W.F., Kidd, R.B., Thomas, E., et al., *Init. Repts. DSDP*, 94 (Pt. 2): Washington (U.S. Govt. Printing Office), 615–634.
- Salimullah, A.R.M., and Stow, D.A.V., 1992. Application of FMS images in poorly recovered coring intervals: examples from ODP Leg 129. In Hurst, A., Griffiths, C.M., and Worthington P.F. (Eds.), *Geological Application of Wireline Logs II*. Geol. Soc. Spec. Publ. London, 65:71–86.
- Sanfilippo, A., and Nigrini, C., 1998. Code numbers for Cenozoic low latitude radiolarian biostratigraphic zones and GPTS conversion tables. *Mar. Micropaleontol.*, 33:109–156.

- Schlumberger, 1989. *Log Interpretation Principles/Applications*: Houston, TX (Schlumberger Educ. Services), SMP-7017.
- , 1994. *IPL Integrated Porosity Lithology* (Schlumberger Wireline and Testing), SMP-9270.
- , 1995. *DSI—Dipole Sonic Imager*: Houston (Schlumberger Wireline and Testing), SMP-5128.
- Schrader, H.J., and Gersonde, R., 1978. Diatoms and silicoflagellates. In Zachariasse, W.J., et al. (Eds.), *Micropaleontological Counting Methods and Techniques: An Exercise of an Eight Metres Section of the Lower Pliocene of Cap Rossello, Sicily*. Utrecht Micropaleontol. Bull., 17:129–176.
- Serra, O., 1984. *Fundamentals of Well-Log Interpretation* (Vol. 1): *The Acquisition of Logging Data*: Dev. Pet. Sci., 15A: Amsterdam (Elsevier).
- , 1986. *Fundamentals of Well-Log Interpretation* (Vol. 2): *The Interpretation of Logging Data*. Dev. Pet. Sci., 15B.
- , 1989. *Formation MicroScanner Image Interpretation*: Houston (Schlumberger Educ. Services), SMP-7028.
- Serra, O., and Sulpice, L., 1975. Sedimentological analysis of shale-sand series from well logs. *Trans. SPWLA 16th Ann. Logging Symp.*, Pap. W.
- Shepard, F., 1954. Nomenclature based on sand-silt-clay ratios. *J. Sediment. Petrol.*, 24:151–158.
- Shipboard Scientific Party, 1992. Explanatory notes. In Davis, E.E., Mottl, M.J., Fisher, A.T., et al., *Proc. ODP, Init. Repts.*, 139: College Station, TX (Ocean Drilling Program), 55–97.
- , 1994. Explanatory notes. In Mountain, G.S., Miller, K.G., Blum, P., et al., *Proc. ODP, Init. Repts.*, 150: College Station, TX (Ocean Drilling Program), 21–42.
- , 1995. Explanatory notes. In Shipley, T.H., Ogawa, Y., Blum, P., et al., *Proc. ODP, Init. Repts.*, 156: College Station, TX (Ocean Drilling Program), 39–68.
- , 1996. Explanatory notes. In Paull, C.K., Matsumoto, R., Wallace, P.J., et al., *Proc. ODP, Init. Repts.*, 164: College Station, TX (Ocean Drilling Program), 13–41.
- , 1997. Explanatory notes. In Lyle, M., Koizumi, I., Richter, C., et al., *Proc. ODP, Init. Repts.*, 167: College Station, TX (Ocean Drilling Program), 15–39.
- , 1999a. Explanatory notes. In Carter, R.M., McCave, I.N., Richter, C., Carter, L., et al., *Proc. ODP, Init. Repts.*, 181, 1–65 [CD-ROM]. Available from: Ocean Drilling Program, Texas A&M University, College Station, TX 77845-9547, U.S.A.
- , 1999b. Explanatory notes. In Gersonde, R., Hodell, D.A., Blum, P., et al., *Proc. ODP, Init. Repts.* 177, 1–57 [CD-ROM]. Available from: Ocean Drilling Program, Texas A&M University, College Station, TX 77845-9547, U.S.A.
- Spiegler, D., 1991. Occurrence of *Bolboforma* (algae, Chrysophyta) in the subantarctic (Atlantic) Paleogene. In Ciesielski, P.F., Kristoffersen, Y., et al., *Proc. ODP, Sci. Results*, 114: College Station, TX (Ocean Drilling Program), 325–334.
- , 1999. *Bolboforma* biostratigraphy from the Hatton–Rockall Basin (North Atlantic). In Raymo, M.E., Jansen, E., Blum, P., and Herbert, T.D. (Eds.), 1999. *Proc. ODP, Sci. Results*, 162: College Station, TX (Ocean Drilling Program), 35–49.
- Stott, L.D., and Kennett, J.P., 1990. Antarctic Paleogene planktonic foraminifer biostratigraphy: ODP Leg 113, Sites 689 and 690. In Barker, P.F., Kennett, J.P., et al., *Proc. ODP, Sci. Results*, 113: College Station, TX (Ocean Drilling Program), 549–569.
- Takemura, A., 1992. Radiolarian Paleogene biostratigraphy in the southern Indian Ocean, Leg 120. In Wise, S.W., Jr., Shlich, R., et al., *Proc. ODP, Sci. Results*, 120: College Station, TX (Ocean Drilling Program), 735–756.
- Takemura, A., and Ling, H.Y., 1997. Eocene and Oligocene radiolarian biostratigraphy from the Southern Ocean: correlation of ODP Legs 114 (Atlantic Ocean) and 120 (Indian Ocean). *Mar. Micropaleontol.*, 30:97–116.
- Tappan, H., 1980. *The Paleobiology of Plant Protists*: San Francisco (W.H. Freeman).
- Timur, A., and Toksöz, M.N., 1985. Downhole geophysical logging. *Annu. Rev. Earth Planet. Sci.*, 13:315–344.
- Tittman, J., 1986. *Geophysical Well Logging*: London (Academic Press).

- Tjalsma, R.C., and Lohmann, G.P., 1983. Paleocene-Eocene bathyal and abyssal benthic foraminifera from the Atlantic Ocean. *Micropaleontol. Spec. Publ.*, 4.
- Truswell, E.M., 1997. Palynomorph assemblages from marine Eocene sediments on the west Tasmanian continental margin and the South Tasman Rise. *Aust. J. Earth Sci.*, 44:633–654.
- van Morkhoven, F.P.C.M., Berggren, W.A., and Edwards, A.S., 1986. Cenozoic cosmopolitan deep-water benthic foraminifera. *Bull. Cent. Rech. Explor.—Prod. Elf-Aquitaine*, 11.
- Wei, W., and Wise, S.W., Jr., 1992. Eocene-Oligocene calcareous nannofossil magneto-biochronology of the Southern Ocean. *Newsl. Stratigr.*, 26:119–132.
- Williams, G.L., Brinkhuis, H., et al., 1998a. Cenozoic dinocyst events. In De Gracianski, et al. (Eds.), *Sequence Stratigraphy of European Basins*. Spec. Publ.—Soc. Econ. Paleontol. Mineral., 60.
- Williams, G.L., Lentin, J.K., and Fensome, R.A., 1998b. The Lentin and Williams Index of fossil dinoflagellate cysts, 1998 edition. *Am. Assoc. Stratigr. Palynol., Contrib. Ser.*, 34.
- Wilson, G.J., 1984. New Zealand Late Jurassic to Eocene dinoflagellate biostratigraphy: a summary. *Newsl. Stratigr.*, 13:104–117.
- , 1988. Paleocene and Eocene dinoflagellate cysts from Waipawa, Hawkes Bay, New Zealand. *N.Z. Geol. Surv. Paleontol. Bull.*, 57.
- , 1989. Marine palynology. In Barrett, P.J. (Ed.), *Antarctic Cenozoic History from the CIROS-1 Drillhole, McMurdo Sound*. N.Z. Dep. Sci. Ind. Res. Bull, 245:129–133.
- Wilson, W.D., 1960. Speed of sound in seawater as a function of temperature, pressure and salinity. *J. Acoust. Soc. Am.*, 32:641–644.
- Wrenn, J.H., and Hart, G.F., 1988. Paleogene dinoflagellate cyst biostratigraphy of Seymour Island, Antarctica. *Mem.—Geol. Soc. Am.*, 169:321–447.
- Wyllie, M.R.J., Gregory, A.R., and Gardner, L.W., 1956. Elastic wave velocities in heterogeneous and porous media. *Geophysics*, 21:41–70.

Figure F1. Coring and depth intervals.



 Represents recovered material

BOTTOM FELT: distance from rig floor to seafloor

TOTAL DEPTH: distance from rig floor to bottom of hole (sub-bottom bottom)

PENETRATION: distance from seafloor to bottom of hole (sub-bottom bottom)

NUMBER OF CORES: total of all cores recorded, including cores with no recovery

TOTAL LENGTH OF CORED SECTION: distance from sub-bottom top to sub-bottom bottom minus drilled (but not cored) areas in between

TOTAL CORE RECOVERED: total from adding a, b, c, and d in diagram

CORE RECOVERY (%): equals TOTAL CORE RECOVERED divided by TOTAL LENGTH OF CORED SECTION times 100

Figure F2. Examples of numbered core sections.

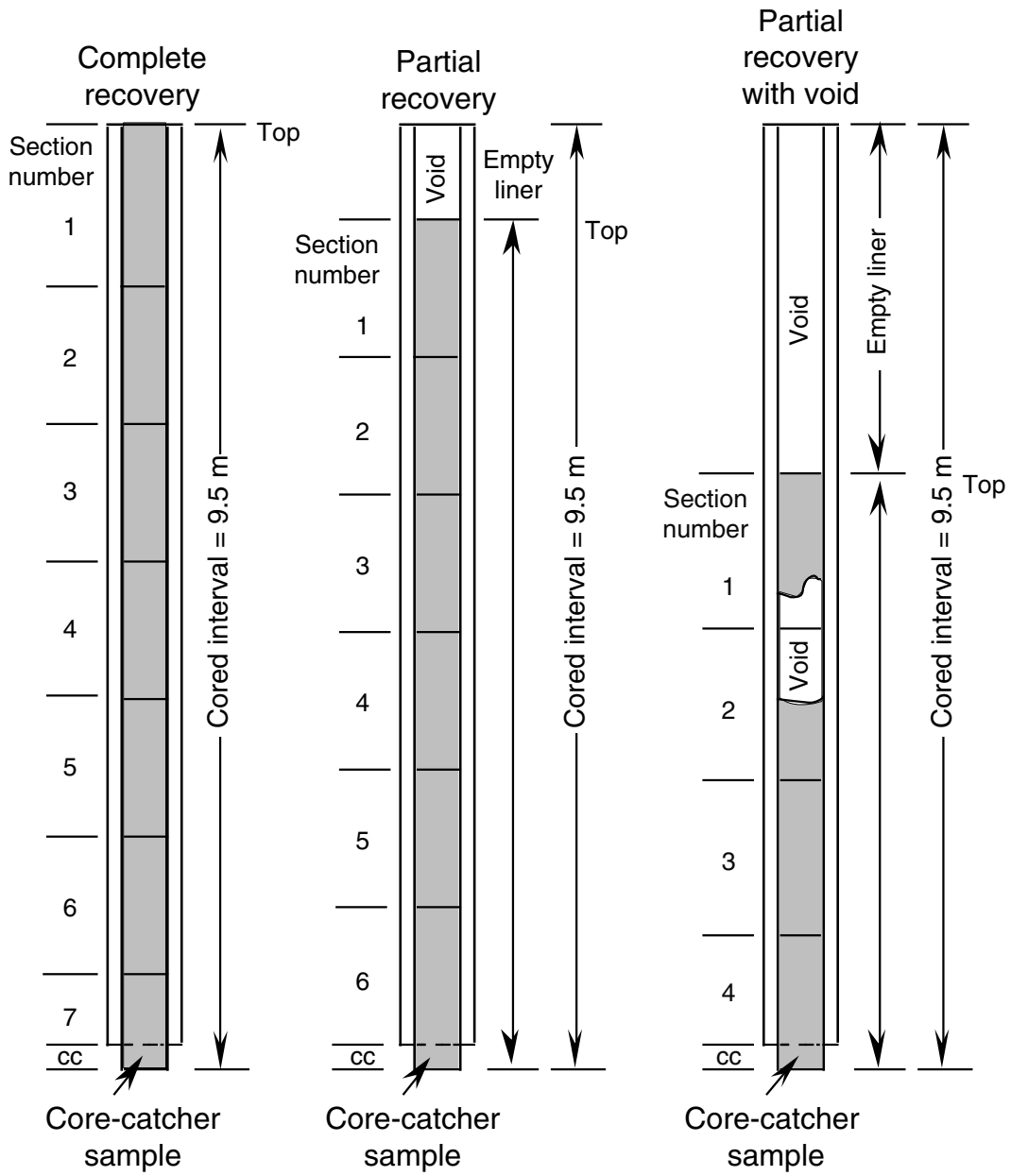


Figure F3. Key to symbols used to represent lithology, sedimentary structures, accessories, bioturbation, and drilling disturbance in the barrel sheets from Leg 189. The bioturbation indexes ii1 to ii5 are from Drosler and Bottjer (1986).

Lithologies

	Limestone		Sand
	Nannofossil ooze		Silty sand
	Foraminifer ooze		Clayey sand
	Nannofossil chalk		Silt/siltstone
	Foraminiferal chalk		Sandy silt
	Diatom ooze		Clayey silt
	Radiolarian ooze		Clay
	Chert		Sandy clay
	Core void		Silty clay

Drilling disturbances

	Soupy	Slight Moderate Extreme
	Disturbed	
	Flow-in	
	Fractured	
	Biscuits	
	Breccia	

Lithologic accessories

	Abrupt contact		Pyrite nodule
	Gradational contact		Pyrite
	Laminae		Glauconite
	Isolated laminae		Wood
	Fluid escape structure		Slump
	Coarser interval		Convolute bedding
	Breccia (lithologic tool)		Cross bedding
	Mottled-		Low-angle tabular bedding
	Nodule		Microfault, reverse
	MOTTLED		

Trace and body fossils

	<i>Zoophycos</i>
	<i>Chondrites</i>
	Undefined burrow
	Bivalve
	Solitary coral
	Shell fragment
	Vertebra
	Mollusc
	Gastropods
	Helminthopsis

Bioturbation

Abundant (ii5)	Common (ii4)	Present (ii3)	Rare (ii2)	Absent (ii1)

Figure F4. A. Classification of the whole-rock composition scheme used for Leg 189. Fifty percent of whole-rock composition = lithology; 10%–25% of whole-rock composition = minor modifier, and >25%–50% of whole-rock composition = major modifier. If whole-rock composition is >50% siliciclastic, siliciclastic texture to determine the lithology is applied. B. Textural classification scheme for siliciclastics, modified from Shepard (1954), by subdivision of the central triangular field into sandy clay, silty clay, sandy silt, clayey silt, clayey sand, and silty sand.

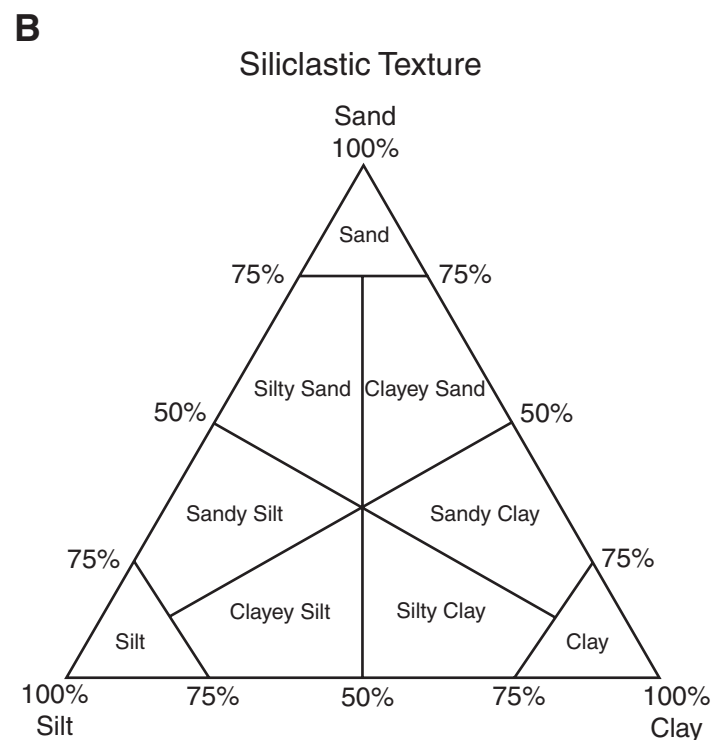
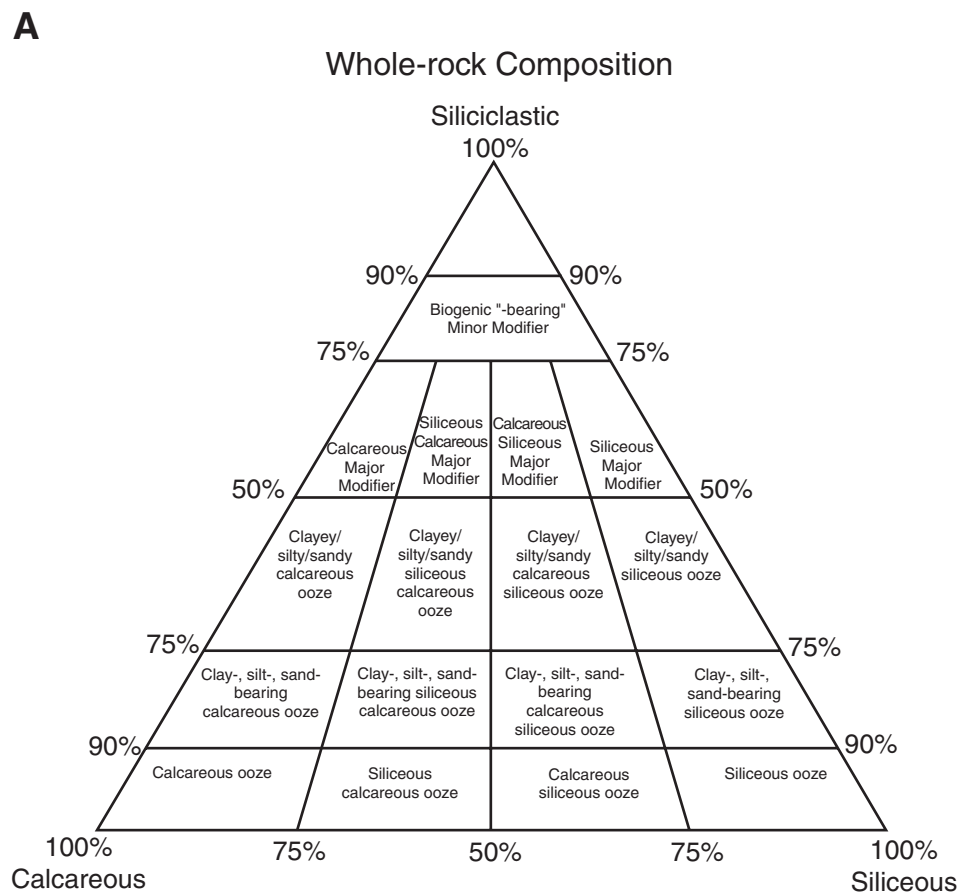


Figure F5. The planktonic foraminiferal bioevents and the zonal schemes used.

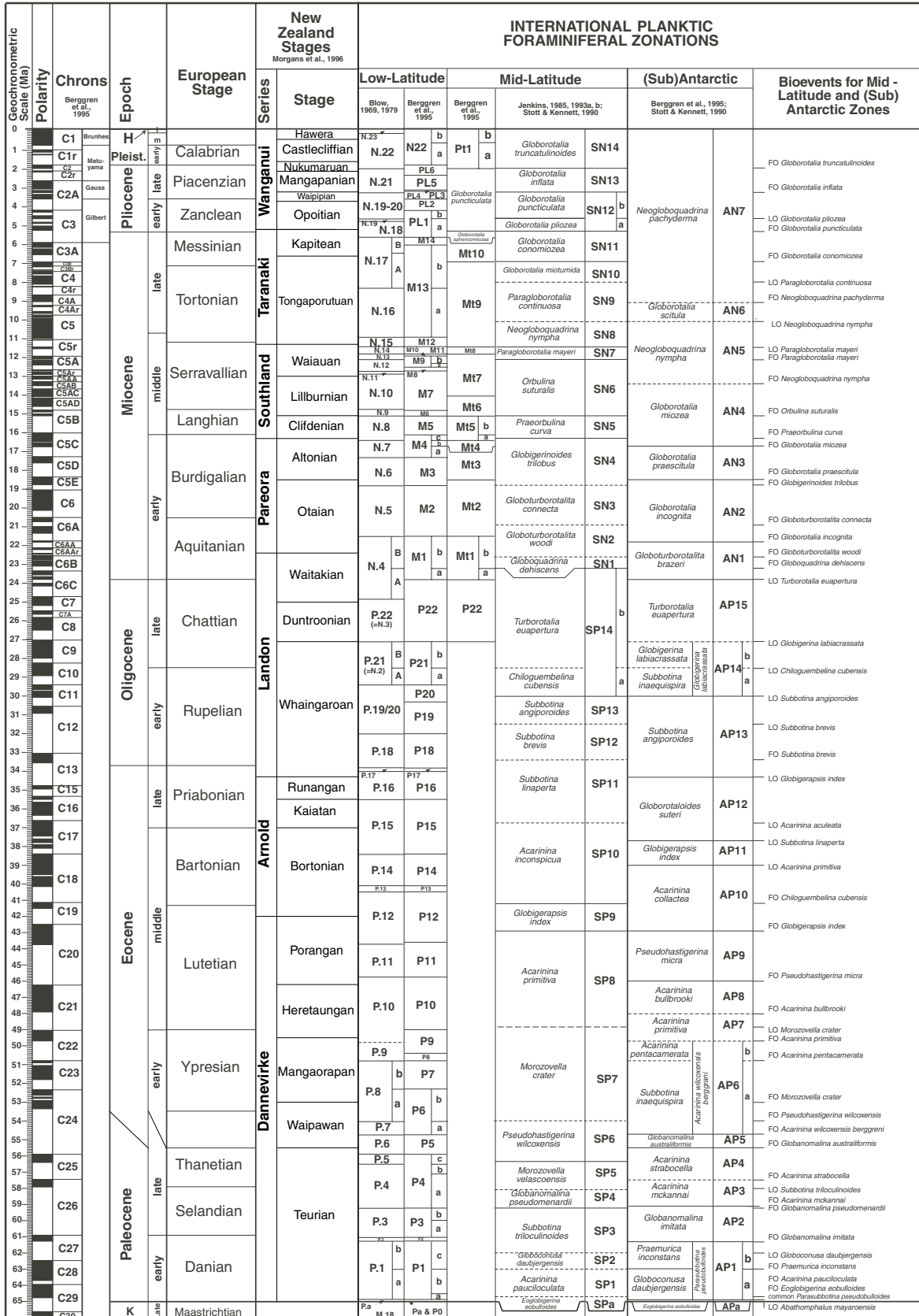


Figure F6. Diatom species ranges used in Leg 189 (compiled from Gersonde et al., 1998, and Shipboard Scientific Party, 1999b).

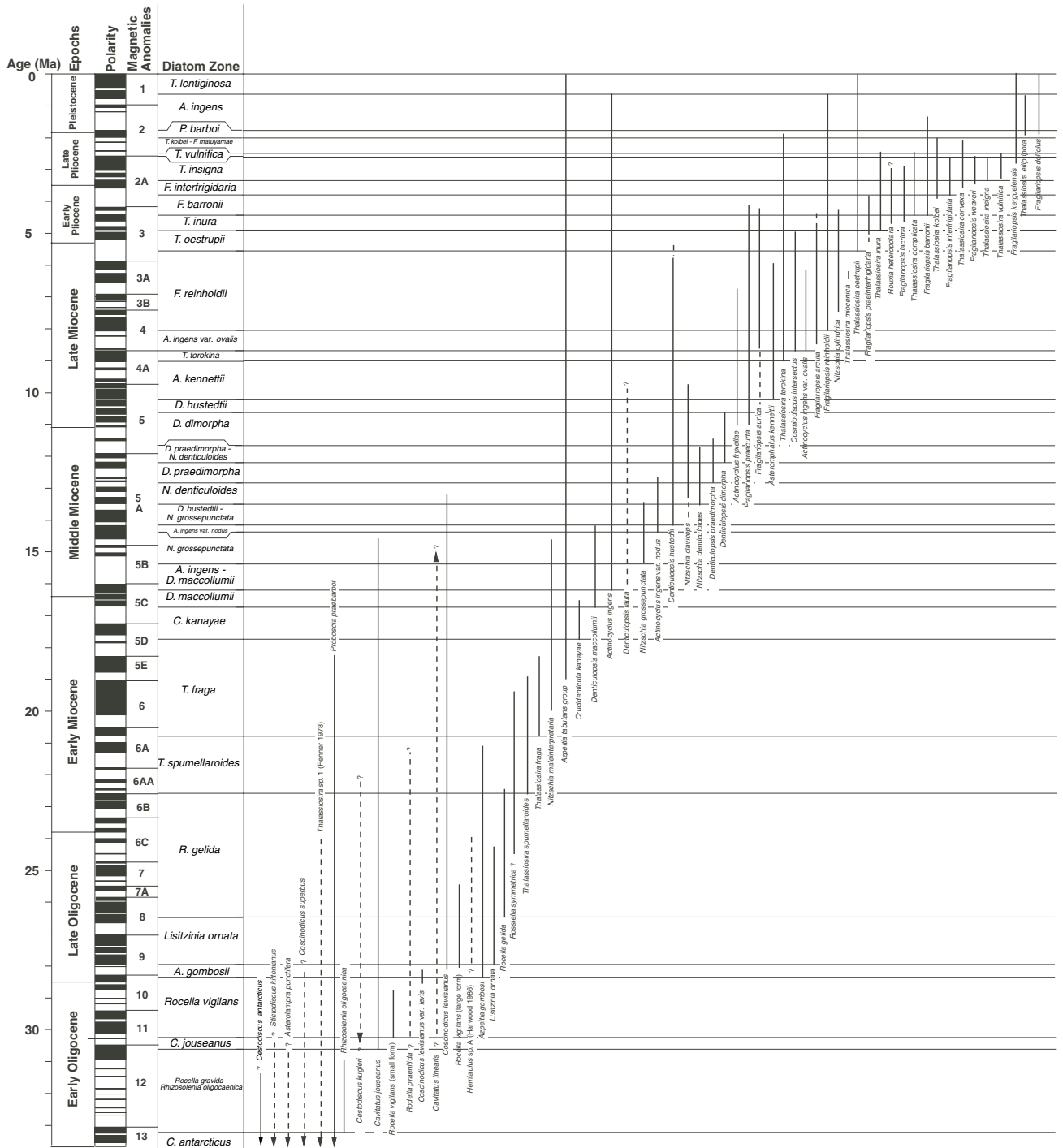


Figure F8. Magnetic orientation convention.

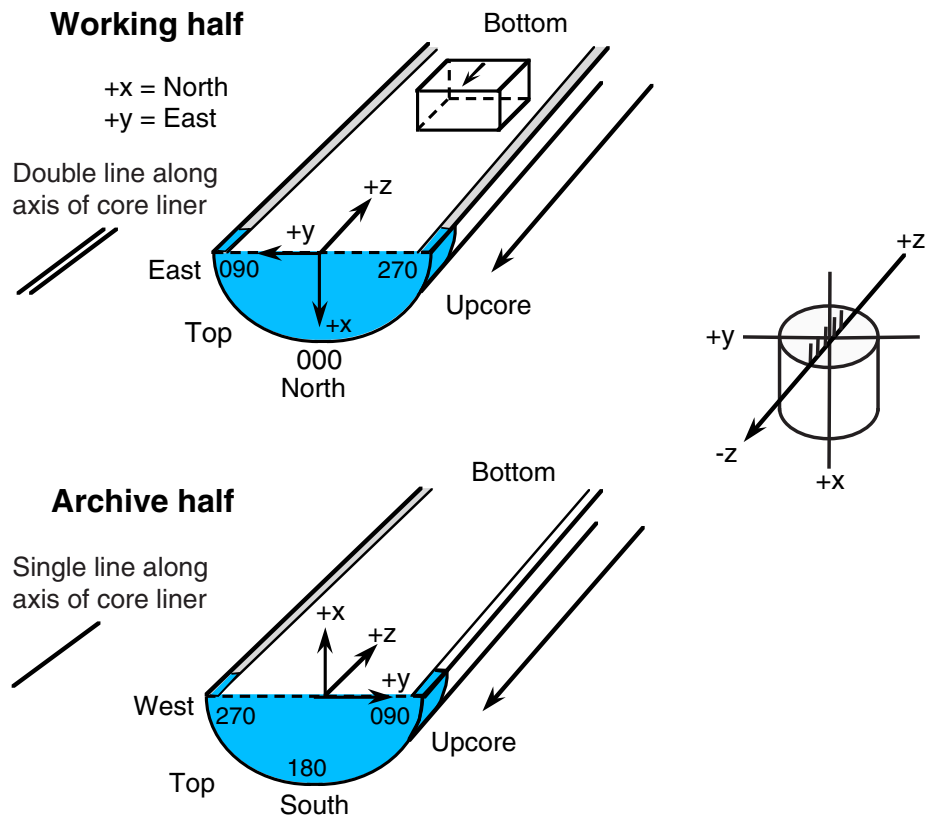


Figure F9. Portions of the GRA bulk density records from Site 1171. Data from each hole are smoothed (21 cm Gaussian) and offset by a constant for clarity. **A.** Cores from Holes 1171A (solid line), 1171B (dotted dashed line), and 1171C (dashed line) on the mbsf depth scale. **B.** The same cores on the meters composite depth (mcd) scale. The composite depth section has the advantage that features common to all holes are in relative alignment. **C.** The spliced GRA bulk density record assembled from the same Site 1171 cores shown in the left and middle panels. In this example, Hole 1171A was used as the backbone. Intervals from Holes 1171B and 1171C were used to cover gaps present in the Hole 1171A record.

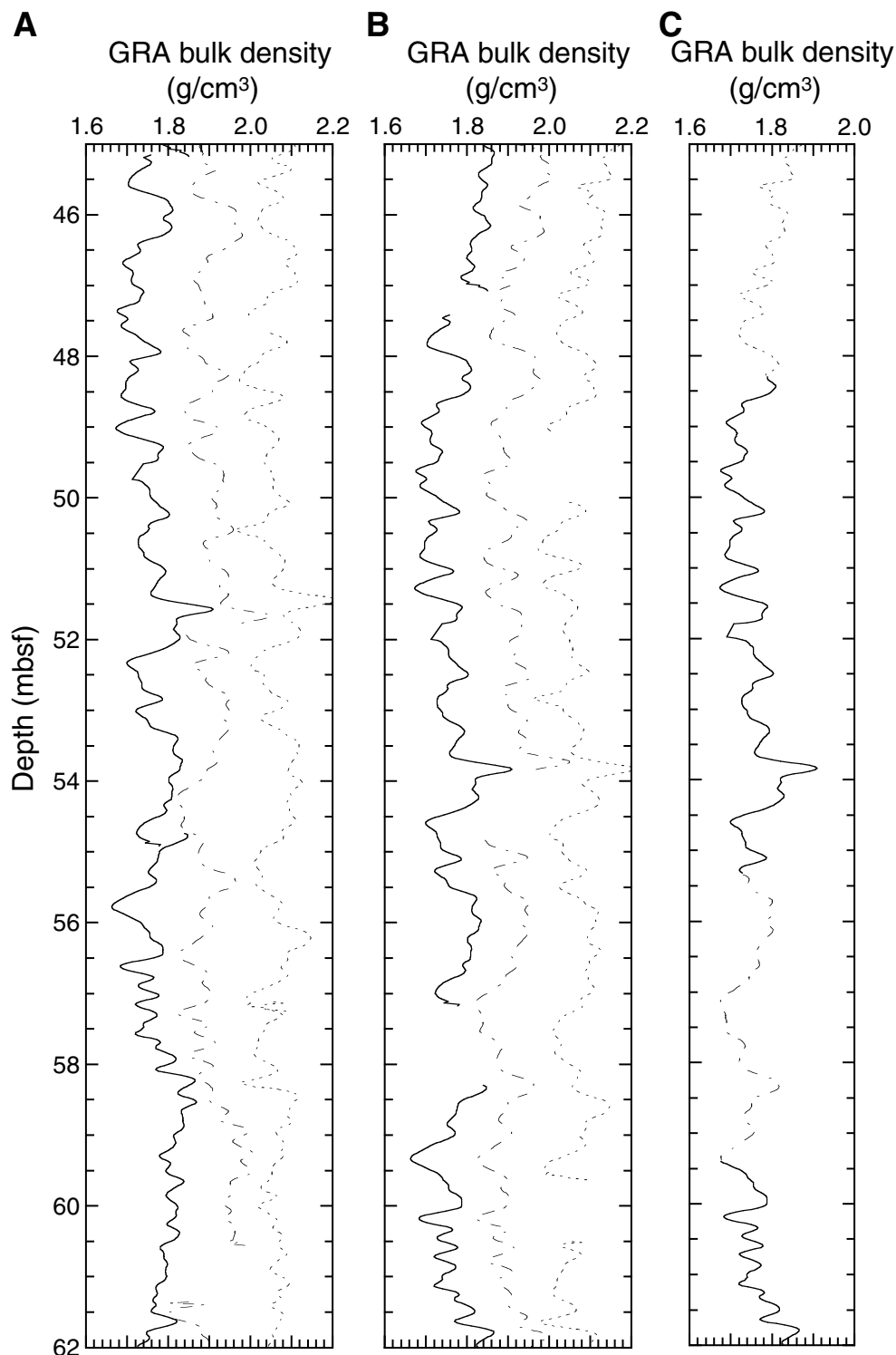


Figure F10. Wireline tool strings used during Leg 189.

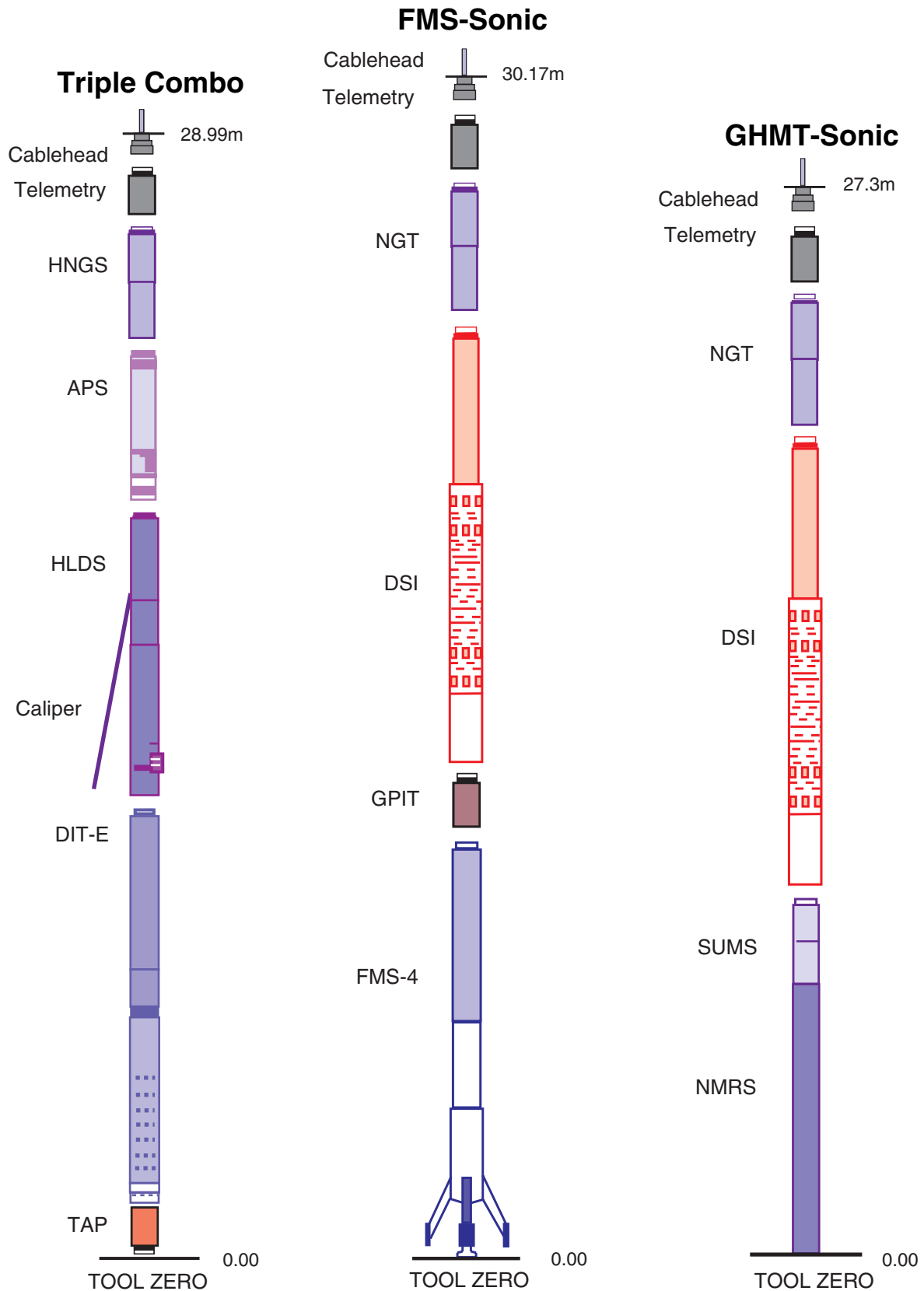


Figure F11. The dipole shear sonic imager.

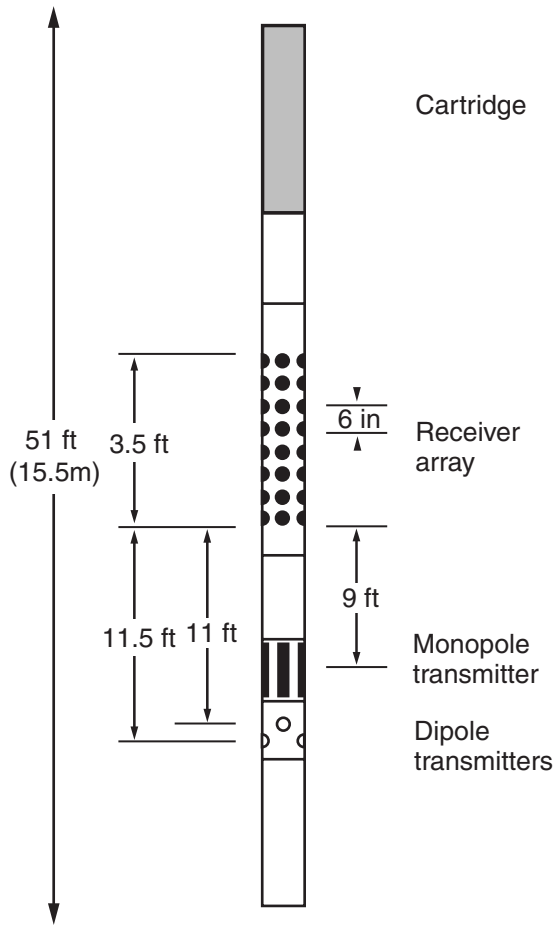


Figure F12. Schematic diagram of the Formation MicroScanner (adapted from Lovell et al., 1998).

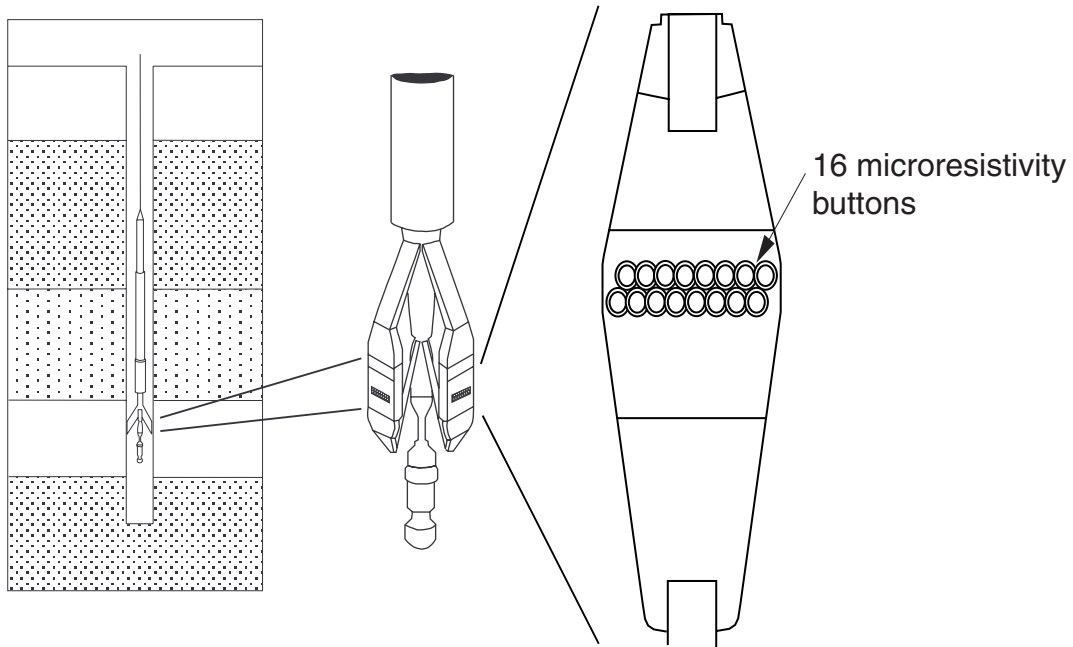


Table T1. Ages of calcareous nannofossil bioevents.

Taxon	Event	Age (Ma)	Taxon	Event	Age (Ma)
<i>E. huxleyi</i>	Acme	0.1	<i>D. druggii</i>	FO	23.2
<i>E. huxleyi</i>	FO	0.3	<i>D. bisectus</i>	LO	23.8
<i>P. lacunosa</i>	LO	0.5	<i>S. ciperoensis</i>	LO	24.0
<i>H. sellii</i>	LO	1.26-1.44	<i>S. distensus</i>	LO	27.0
<i>C. macintyreii</i>	LO	1.6-1.64	<i>S. ciperoensis</i>	FO	28.6
<i>D. brouweri</i>	LO	2.0	<i>D. bisectus</i>	LO	23.9
<i>D. pentaradiatus</i>	LO	2.4	<i>S. delphix</i>	FO	24.3
<i>D. surculus</i>	LO	2.5	<i>Z. bijugatus</i>	LO	24.5
<i>D. tamalis</i>	LO	2.7	<i>S. ciperoensis</i>	LO	24.8
<i>R. pseudoumbilica</i>	LO	3.7	<i>C. altus</i>	LO	26.1
<i>A. tricorniculatus</i>	LO	3.9	<i>S. umbrellus</i>	FO	27.5
<i>D. asymmetricus</i>	FO	4.3	<i>S. distensus</i>	LO	27.5
<i>A. primus</i>	LO	4.6	<i>S. predistensus</i>	LO	27.5
<i>C. rugosus</i>	LO	4.7	<i>S. pseudoradians</i>	LO	29.1
<i>C. acutus</i>	LO	4.9	<i>S. ciperoensis</i>	FO	29.9
<i>C. acutus</i>	FO	5.2	<i>C. abisectus</i>	FO	31.2
<i>D. quinquerramus</i>	LO	5.6	<i>S. distensus</i>	FO	31.5-33.1
<i>A. amplificus</i>	LO	6.0	<i>R. umbilica</i>	LO	31.3-32.3
<i>A. amplificus</i>	FO	6.6	<i>I. recurvus</i>	LO	31.8-33.1
<i>A. delicatus</i>	LO	6.9	<i>E. formosa</i>	LO	32.8-39.7
<i>A. primus</i>	FO	7.2	<i>C. subdistichus</i>	Acme	33.3
<i>D. loeblichii</i>	LO	7.4	<i>R. oamaruensis</i>	LO	33.7
<i>M. conwallis</i>	LO	7.8	<i>D. saipanensis</i>	LO	34.2-35.4
<i>D. berggrenii</i>	FO	8.6	<i>D. barbadensis</i>	LO	34.3-39.0
<i>D. loeblichii</i>	FO	8.7	<i>R. reticulata</i>	LO	35.0-36.1
<i>D. bollii</i>	FO	9.4	<i>R. oamaruensis</i>	FO	35.4
<i>M. conwallis</i>	FO	9.5	<i>I. recurvus</i>	FO	36.0
<i>D. hamatus</i>	LO	9.4	<i>C. oamaruensis</i>	FO	37.0
<i>C. coalitus</i>	LO	9.7	<i>C. grandis</i>	LO	37.1
<i>C. calyculus</i>	FO	10.7	<i>D. bisectus</i>	FO	38.0
<i>D. hamatus</i>	FO	10.7-11.2	<i>C. solitus</i>	LO	40.4
<i>C. miopelagicus</i>	FO	11.0	<i>R. reticulata</i>	FO	42.0
<i>C. coalitus</i>	FO	10.9-11.3	<i>N. fulgens</i>	LO	43.1
<i>D. kugleri</i>	LO	11.5	<i>R. gladius</i>	LO	43.4
<i>D. kugleri</i>	FO	11.8	<i>R. umbilica</i>	FO	43.7
<i>T. rugosus</i>	FO	13.2	<i>C. gigas</i>	LO	44.5
<i>S. heteromorphous</i>	LO	13.6	<i>C. gigas</i>	FO	46.1
<i>H. ampliapertura</i>	LO	15.6	<i>N. fulgens</i>	FO	47.3
<i>S. heteromorphous</i>	FO	18.2	<i>R. inflata</i>	FO	48.5
<i>S. belemnos</i>	LO	18.3	<i>D. subladoensis</i>	FO	49.7
<i>S. belemnos</i>	FO	19.2	<i>A. cymbiformis</i>	LO	65.0
<i>S. conicus</i>	LO	21.8	<i>E. turriseiffelii</i>	LO	65.0

Note: FO = first occurrence, LO = last occurrence.

Table T2. Ages of planktonic foraminiferal bioevents.

Event	Taxon	Age (Ma)
FO	<i>Globorotalia truncatulinoides</i>	1.96
FO	<i>Globorotalia inflata</i>	3.20
LO	<i>Globorotalia pliozea</i>	4.60
FO	<i>Globorotalia puncticulata</i>	5.30
FO	<i>Globorotalia conomiozea</i>	6.90
LO	<i>Paragloborotalia continuosa</i>	8.00
LO	<i>Neogloboquadrina nymphea</i>	10.10
LO	<i>Paragloborotalia mayeri</i>	11.40
FO	<i>Paragloborotalia mayeri</i>	12.10
FO	<i>Orbulina suturalis</i>	15.10
FO	<i>Praeorbulina glomerosa curva</i>	16.30
FO	<i>Globigerinoides trilobus</i>	18.80
FO	<i>Globoturborotalita connecta</i>	20.90
FO	<i>Globoturborotalita woodi</i>	22.60
FO	<i>Globoquadrina dehiscens</i>	23.20
LO	<i>Chiloguembelina cubiensis</i>	28.50
LO	<i>Subbotina angiporoides</i>	30.00
LO	<i>Subbotina brevis</i>	33.50
FO	<i>Subbotina brevis</i>	34.80
LO	<i>Acarinina aculeata</i>	36.00
FO	<i>Chiloguembelina cubiensis</i>	41.20
FO	<i>Globigerapsis index</i>	42.90
LO	<i>Morozovella crater</i>	42.60
FO	<i>Morozovella crater</i>	53.00
FO	<i>Pseudohastigerina wilcoxensis</i>	54.60
FO	<i>Globanomalina pseudomenardii</i>	59.20
LO	<i>Globoconusa daubjergensis</i>	62.00
FO	<i>Praemurica inconstans</i>	63.00
FO	<i>Acarinina pauciloculata</i>	64.70
FO	<i>Eoglobigerina eobulloides</i>	65.00

Note: FO = first occurrence, LO = last occurrence.

Table T3. Ages of diatom bioevents.

Zone	Reference	Top (Ma)	Base (Ma)	Definition of zone base
<i>Thalassiosira lentiginosa</i> c	1	0.00	0.18	<i>H. karstenii</i> LCO
<i>Thalassiosira lentiginosa</i> b	1	0.18	0.42	<i>H. karstenii</i> FCO
<i>Thalassiosira lentiginosa</i> a	1	0.42	0.65	<i>A. ingens</i> LO
<i>Actinocyclus ingens</i> c	1	0.65	1.07	<i>T. elliptipora</i> FCO
<i>Actinocyclus ingens</i> b	1	1.07	1.30	<i>F. barronii</i> LO
<i>Actinocyclus ingens</i> a	1	1.30	1.80	<i>P. barboi</i> LO
<i>Proboscia barboi</i>	1	1.77	2.00	<i>T. kolbei</i> LO, (<i>F. matuyamae</i> FO 2.1 Ma for northern sites)
<i>Thalassiosira kolbei</i> / <i>Fragilariopsis matuyamae</i>	1	2.00 (2.10)	2.50	<i>F. matuyamae</i> FCO, <i>T. vulnifica</i> LO
<i>Thalassiosira vulnifica</i>	1	2.50	2.63	<i>F. interfrigidaria</i> LO, <i>T. insigna</i> LO
<i>Thalassiosira insigna</i>	2	2.63	3.26	<i>T. vulnifica</i> FO
<i>Fragilariopsis interfrigidaria</i>	2	3.26	3.80	<i>F. interfrigidaria</i> FO
<i>Fragilariopsis barronii</i>	2	3.80	4.44	<i>F. barronii</i> FO, <i>T. complicata</i> FO
<i>Thalassiosira inura</i>	2	4.44	4.92	<i>T. inura</i> FO
<i>Thalassiosira oestrupii</i>	2	4.92	5.56	<i>T. oestrupii</i> FO
<i>Fragilariopsis reinholdii</i>	2	5.56	8.10	<i>F. reinholdii</i> FO
<i>Actinocyclus ingens</i> var. <i>ovalis</i>	2	8.10	8.68	<i>C. intersectus</i> FO, <i>A. ingens</i> var. <i>ovalis</i> FO
<i>Thalassiosira torokina</i>	2	8.68	9.01	<i>T. torokina</i> FO
<i>Asteromphalus kennettii</i>	2	9.01	10.23	<i>A. kennettii</i> FO
<i>Denticulopsis hustedtii</i>	2	10.23	10.63	<i>D. dimorpha</i> LO
<i>Denticulopsis dimorpha</i>	2	10.63	11.67	<i>N. denticuloides</i> LO
<i>Denticulopsis dimorpha</i> / <i>Nitzschia denticuloides</i>	2	11.67	12.20	<i>D. dimorpha</i> FO
<i>Denticulopsis praedimorpha</i>	2	12.20	12.84	<i>D. praedimorpha</i> FO
<i>Nitzschia denticuloides</i>	2	12.84	13.51	<i>N. grossepunctata</i> LO, <i>N. denticuloides</i> FO
<i>Denticulopsis hustedtii</i> / <i>Nitzschia grossepunctata</i>	2	13.51	14.17	<i>D. hustedtii</i> FO
<i>Actinocyclus ingens</i> var. <i>nodus</i>	2	14.17	14.38	<i>A. ingens</i> var. <i>nodus</i> FO
<i>Nitzschia grossepunctata</i>	2	14.38	15.38	<i>N. grossepunctata</i> FO
<i>Actinocyclus ingens</i> / <i>Denticulopsis maccollumii</i>	2	15.38	16.20	<i>A. ingens</i> FO
<i>Denticulopsis maccollumii</i>	2	16.20	16.75	<i>D. maccollumii</i> FO
<i>Crucidentacula kanayae</i>	2	16.75	17.72	<i>C. kanayae</i> FO
<i>Thalassiosira fraga</i>	2	17.72	20.79	<i>T. fraga</i> FO
<i>Thalassiosira spumellaroides</i>	2	20.79	22.58	<i>T. spumellaroides</i> FO
<i>Rocella gelida</i>	2	22.58	26.50	<i>R. gelida</i> FO
<i>Lisitzinia ornata</i>	2	26.50	27.95	<i>L. ornata</i> FO
<i>Azpeitia gombosi</i>	2	27.95	28.35	<i>A. gombosi</i> FO
<i>Rocella vigilans</i>	2	28.35	30.24	<i>R. vigilans</i> (small) FO
<i>Cavitatus jouseanus</i>	2	30.24	30.62	<i>C. jouseanus</i> FO
<i>Rhizosolenia gravida</i> / <i>oligocaenica</i>	2	30.62	33.22	<i>R. oligocaenica</i> FO

Notes: 1 = Gersonde and Bárcena (1998), 2 = Shipboard Scientific Party (1999a). LCO = last consistent occurrence, FCO = first consistent occurrence, LO = last occurrence, FO = first occurrence.

Table T4. Ages of radiolarian bioevents.

Event	Taxon name	Age (Ma)	Source of datum
FO	<i>Stylatractus</i> sp. A of Nakaseko and Nishimura (1982)		
LO	<i>Stylatractus universus</i> Hays	0.45	McIntyre and Kaczmarska (1996)
LO	<i>Antarctissa cylindrica</i> Petrushevskaya	0.65	Caulet (1991)
LO	<i>Pterocarnium charybdeum trilobum</i> (Haeckel)	0.88	Lazarus (1992)
LO	<i>Eucyrtidium calvertense</i> Haeckel	1.90	Lazarus (1992)
LO	<i>Helotholus vema</i> Hays	2.40	Ramsay and Baldauf (1999)
LO	<i>Prunopyle titan</i> Campbell et Clark	3.48	Caulet (1991)
LO	<i>Desmospyris spongia</i> Hays	2.46	Caulet (1991)
LO	<i>Lampromitra coronata</i> Haeckel	3.35	Lazarus (1992)
FO	<i>Helotholus vema</i> Hays	4.50	Ramsay and Baldauf (1999)
LCO	<i>Lychnocanoma grande</i> (Campbell et Clark)	5.00	Lazarus (1992)
LO	<i>Amphymenium challengeriae</i> Weaver	6.10	Lazarus (1992)
FO	<i>Amphymenium challengeriae</i> Weaver	6.60	Recalculated
FO	<i>Acrosphaera</i> (?) <i>labrata</i> Lazarus	7.80	Lazarus (1992)
LO	<i>Cycladophora spongothorax</i> (Hays)	9.10	Lazarus (1992)
ET	<i>A. murrayana</i> (Haeckel) → <i>A. australis</i> Lazarus	10.40	Lazarus (1992)
FO	<i>Eucyrtidium pseudoinflatum</i> Weaver	10.60	Lazarus (1992)
LO	<i>Actinomma golownini</i> Petrushevskaya	10.80	Lazarus (1992)
FO	<i>Cycladophora spongothorax</i> (Hays)	12.14	Lazarus (1992)
FO	<i>Dendrospyris megalcephalis</i> Chen	12.78	Lazarus (1992)
FO	<i>Actinomma golownini</i> Petrushevskaya	13.22	Lazarus (1992)
FO	<i>Cycladophora humerus</i> (Petrushevskaya)	14.18	Abelmann (1990)
FO	<i>Eucyrtidium punctatum</i> Ehrenberg	17.03	Abelmann (1990)
FO	<i>Cycladophora golli regipileus</i> (Chen)	19.10	Abelmann (1990)
FO	<i>Theocorys longithorax</i> Petrushevskaya	20.65	Abelmann (1990)
FO	<i>Cycladophora antiqua</i> Abelmann	21.95	Abelmann (1990)
FO	<i>Cyrtocapsella tetrapera</i> (Haeckel)	23.62	Sanfilippo and Nigrini (1998)
LO	<i>Axoprunum</i> (?) <i>irregularis</i> Takemura	32.70	Recalculated
FO	<i>Eucyrtidium antiquum</i> Caulet	32.96	Recalculated
FO	<i>Eucyrtidium spinosum</i> Takemura	37.00	Recalculated
FO	<i>Lithapium mitra</i> (Ehrenberg)	39.00	Recalculated
FO	<i>Eusyringium fistuligerum</i> (Ehrenberg)	42.00	Recalculated
FO	<i>Eusyringium lagena</i> (Ehrenberg)	47.00	Recalculated
FO	<i>Dictyoprora mongolfieri</i> (Ehrenberg)	51.00	Recalculated
LO	<i>Bekoma divaricata</i> Foreman	53.20	Recalculated
ET	<i>Bekoma bidartensis</i> Riedel et Sanfilippo → <i>B. divaricata</i>	54.40	Recalculated
LO	<i>Bekoma campechensis</i> Foreman	55.60	Recalculated
FO	<i>Bekoma campechensis</i> Foreman	58.00	Recalculated
FO	<i>Miscroscidaicapsa</i> (?) sp.	59.70	Recalculated
FO	<i>Buryella tetradica</i> Foreman	60.90	Spencer-Cervato (1999)
FO	<i>Buryella foremanae</i> Petrushevskaya	62.80	Spencer-Cervato (1999)
FO	<i>Buryella granulata</i> (Petrushevskaya)	63.90	Spencer-Cervato (1999)
FO	<i>Amphisphaera kina</i> Hollis	64.60	Spencer-Cervato (1999)
FO	<i>Amphisphaera aotea</i> Hollis	65.10	Spencer-Cervato (1999)

Note: FO = first occurrence, LO = last occurrence, LCO = last consistent occurrence, ET = earliest transition.

Table T5. Composite depth section, Site 1171.

Core	Depth (mbsf)	Offset (m)	Depth (mcd)
189-1171A-			
1H	0.0	0.00	0.00
2H	7.1	0.74	7.84
3H	16.6	0.56	17.16
4H	26.1	1.18	27.28
5H	35.6	1.90	37.50
6H	45.1	2.26	47.36
7H	54.6	3.56	58.16
8H	64.1	4.70	68.80
9H	73.6	5.44	79.04
10H	83.1	5.88	88.98
11H	92.6	6.76	99.36
12H	102.1	6.74	108.84
13X	111.6	6.74	118.34
14X	114.8	6.74	121.54
189-1171B-			
1H	0.0	0.12	0.12
2H	4.3	0.34	4.64
3H	13.8	0.10	13.90
4H	23.3	1.06	24.36
5H	32.8	1.22	34.02
6H	42.3	2.06	44.36
7H	51.8	2.90	54.70
8H	61.3	3.36	64.66
9H	70.8	4.66	75.46
10H	80.3	6.28	86.58
11H	89.8	6.98	96.78
12H	99.3	6.88	106.18
189-1171C-			
1H	0.0	0.44	0.44
2H	9.5	0.74	10.24
3H	19.0	0.02	19.02
4H	28.5	0.34	28.84
5H	38.0	1.60	39.60
6H	47.5	2.38	49.88
7H	57.0	3.38	60.38
8H	66.5	5.38	71.88
9H	76.0	5.40	81.40
10H	85.5	6.22	91.72
11H	95.0	6.94	101.94
12X	104.5	6.68	111.18
13X	110.2	6.68	116.88
14X	115.2	6.68	121.88

Table T6. Splice tie points, Site 1171.

Hole, core, section, interval (cm)	Depth			Hole, core, section, interval (cm)	Depth	
	(mbsf)	(mcd)			(mbsf)	(mcd)
189-				189-		
1171A-1H-4, 112	5.62	5.62	Tie to	1171C-1H-4, 68	5.18	5.62
1171C-1H-7, 6	9.00	9.44	Tie to	1171A-2H-2, 10	8.70	9.44
1171A-2H-6, 106	15.66	16.40	Tie to	1171B-3H-2, 100	16.30	16.40
1171B-3H-3, 90	17.70	17.80	Tie to	1171A-3H-1, 64	17.24	17.80
1171A-3H-5, 72	23.32	23.88	Tie to	1171C-3H-4, 36	23.86	23.88
1171C-3H-5, 92	25.92	25.94	Tie to	1171B-4H-2, 8	24.88	25.94
1171B-4H-6, 8	30.88	31.94	Tie to	1171C-4H-3, 10	31.60	31.94
1171C-4H-4, 140	34.40	34.74	Tie to	1171B-5H-1, 72	33.52	34.74
1171B-5H-4, 10	37.40	38.62	Tie to	1171A-5H-1, 112	36.72	38.62
1171A-5H-3, 122	39.82	41.72	Tie to	1171C-5H-2, 62	40.12	41.72
1171C-5H-6, 118	46.68	48.28	Tie to	1171A-6H-1, 92	46.02	48.28
1171A-6H-6, 46	53.06	55.32	Tie to	1171B-7H-1, 62	52.42	55.32
1171B-7H-4, 18	56.48	59.38	Tie to	1171A-7H-1, 122	55.82	59.38
1171A-7H-6, 28	62.38	65.94	Tie to	1171B-8H-1, 128	62.58	65.94
1171B-8H-6, 92	69.72	73.08	Tie to	1171A-8H-4, 114	68.38	73.08
1171A-8H-7, 8	71.82	76.52	Tie to	1171B-9H-1, 106	71.86	76.52
1171B-9H-4, 144	76.74	81.40	Tie to	1171A-9H-2, 86	75.96	81.40
1171A-9H-5, 122	80.82	86.26	Tie to	1171C-9H-4, 36	80.86	86.26
1171C-9H-6, 90	84.40	89.80	Tie to	1171A-10H-1, 82	83.92	89.80
1171A-10H-6, 74	91.34	97.22	Tie to	1171C-10H-4, 100	91.00	97.22
1171C-10H-5, 128	92.78	99.00	Tie to	1171B-11H-2, 72	92.02	99.00
1171B-11H-4, 6	94.36	101.34	Tie to	1171A-11H-2, 48	94.58	101.34
1171A-11H-6, 16	100.26	107.02	Tie to	1171B-12H-1, 84	100.14	107.02
1171B-12H-3, 144	103.74	110.62	Tie to	1171A-12H-2, 28	103.88	110.62
1171A-12H-6, 96	110.56	117.30				

Table T7. Relative standard deviations for analysis of dissolved species.

Analyte	SD (%)	Replicant
Cl ⁻	<0.2	IAPSO
Alkalinity	1.6	IAPSO and Borax standards
SO ₄ ²⁻	<1.0	Samples
K ⁺	2.9	Samples
Mg ²⁺	<1.0	Samples
Ca ²⁺	2.6	Samples
Li ⁺	1.8	IAPSO
Sr ²⁺	1.2	IAPSO
NH ₄ ⁻	2.7	Samples
H ₄ SiO ₄ ⁰	3.3	Samples

Notes: SD = standard deviation. IAPSO = International Association for the Physical Science of the Ocean.

Table T8. Wireline tool strings used and properties measured.

Tool strings*	Typical logging speed (m/hr)	Individual tools*	Properties measured	Sample interval (cm)	Approximate vertical resolution (cm)	Approximate depth of investigation (cm)
Triple combination (total length ~32 m)	250-275	HNGS	Natural gamma ray	15	45	Variable
		APS	Porosity	5 and 15	30	15
		HLDS	Bulk density, PEF	15	38	15
		DITE-SFL	Resistivity	15	150/90/60	150/76/38
		TAP	Temperature	1/s	NA	NA
			Tool acceleration	4/s		
FMS-sonic (total length ~30 m)	250-275	NGT	Natural gamma ray	15	45	45
		GPIT	Tool orientation	1 or 15		
		DSI	Sonic velocity	15	110	15–30
		FMS	Resistivity image	0.25	0.5	15
GHMT (total length ~9 m)	300-400	NGT	Natural gamma ray	15	45	25
		SUMS	Susceptibility	5 and 15	35	
		NMRS	Total field	5 and 15	45	NA

Notes: * = see Table T9, p. 58, for explanations of acronyms used to describe tool strings and individual tool names. NA = not applicable.

Table T9. Acronyms used for the wireline tool strings and their measurements.

Tool	Output	Explanation	Units
HNCS		Hostile environment natural gamma-ray sonde	
	HSGR	Standard (total) gamma ray	gAPI
	HCGR	Computed gamma ray (HSGR - uranium contribution)	gAPI
	HFK	Formation potassium	Fraction
	HTHO	Thorium	ppm
	HURA	Uranium	ppm
NGT		Natural gamma-ray tool	
	SGR	Standard total gamma ray	gAPI
	CGR	Computed gamma ray (SGR minus uranium contribution)	gAPI
	POTA	Potassium	%
	THOR	Thorium	ppm
	URAN	Uranium	ppm
APS		Accelerator porosity sonde	
	APLC	Near array porosity (limestone corrected)	Fraction
	FPLC	Far array porosity (limestone corrected)	Fraction
	SIGF	Neutron capture cross section of the formation (Sf)	Formation capture cross section (CU)
	STOF	Tool standoff (computed distance from borehole wall)	In
HLDS		High-temperature lithodensity sonde	
	RHOM	Bulk density (corrected)	g/cm ³
	PEFL	Photoelectric effect	barn/e ⁻
	LCAL	Caliper - measure of borehole diameter	In
	DRH	Bulk density correction	g/cm ³
DIT		Dual induction tool	
SFR		Spherically focused resistivity	
	IDPH	Deep Induction phasor-processed resistivity	Ωm
	IMPH	Medium induction phasor-processed resistivity	Ωm
	SFLU	Shallow spherically focused resistivity	Ωm
GHMT		Geologic magnetic tool	
	MAGS	Magnetic susceptibility (limited range)	ppm
	RMGS	Low resistivity magnetic susceptibility (wider range)	ppm
	MAGC	Earth conductivity	ppm
	MAGB	Earth total magnetic field	nT
DSI		Dipole shear sonic imager	
	DTCO	Compressional wave transit time	μs/ft
	DTSM	Shear wave transit time	μs/ft
	DTST	Stoneley wave transit time	μs/ft
TAP		High resolution temperature/acceleration/pressure tool	°C, m/s ² , psi
GPIT		General purpose inclinometer cartridge	
	FX, FY, FZ	Magnetic field (3 orthogonal directions)	nT
	AX, AY, AZ	Acceleration (3 orthogonal directions)	m/s ²

Note: gAPI = American Petroleum Institute measurement for gamma ray.

CHAPTER NOTES*

- N1. 16 May 2001—Erratum: The spelling of McGonigal has been corrected.
- N2. 16 May 2001—Erratum: The reference to *ODP Tech. Note 29* was originally cited in two formats. This version contains the correct citation.